Chapter 3

Electron track reconstruction

Electron's path through the ATLAS detector is marked by a track in the inner detector (ID) and a cluster in the EM calorimeter (ECAL). ATLAS's arsenal for electron identification consists of two independent weapons. The first one is matching the ID track to its associated ECAL cluster. Position matching is expected to be approximately independent of the energy, while E_T/p_T matching depends crucially on transverse energy, as the tracker resolution is degrading with increasing p_T and the accuracy of the energy measurement in the ECAL is improving. The second weapon is the transition radiation (TR) function of the TRT. As electrons are the lightest particles and transition radiation intensity depends linearly on the relativistic γ factor ($I_{\mathrm{TR}} \propto \gamma$), a higher signal is expected in the TRT from electrons than from other particles. On average, approximately 25% of the TRT hits are above the TR threshold for electrons (less than 10% for pions).

The first section of this chapter presents the electron reconstruction problems in full detail. In the following sections an appropriate algorithm for electron track reconstruction is presented and its efficiency and performance analysed.

3.1 Pitfalls in electron reconstruction

Electrons at the LHC energy scale are plagued by bremsstrahlung effects giving one trying to reconstruct them faithfully a most nightmarish time. The situation in general can be best summarized by the material distribution in the ATLAS inner detector (Fig:3.1) and the following points:

1. **the p_T resolution** is deteriorated due to radiation losses proportional to the amount of material traversed, but the curvature precision gets better with more measurements and improves quadratically with the track length. These two effects are of course in direct contradiction.

2. **The reconstruction efficiency** is sacrificed by the cuts required to retain resolution and to suppress fakes. Some well reconstructed tracks can get killed by blunt cuts even though their identity can be established unambiguously.

3. E_T/p_T **matching** for $e^{\pm}$ identification can be very misleading. In the case of a disastrous early bremsstrahlung, a method of the position matching of the track and EM cluster provides a better way of electron identification.

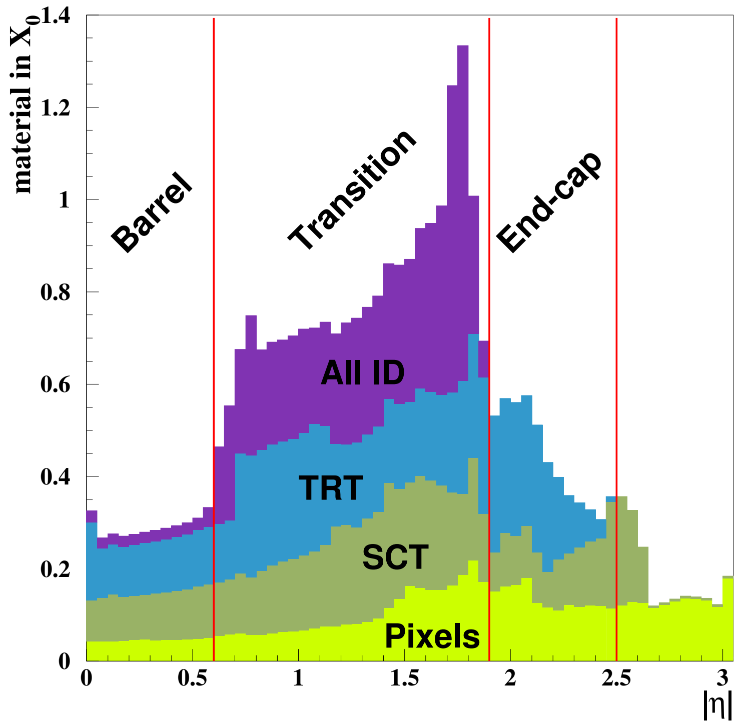

Figure 3.1: Distribution of the material in radiation length units versus $|\eta|$. Amount of material for each sub-detector is plotted in a cumulative way. Red lines separate the $|\eta|$ regions used in analysis.

The objective of this preliminary study was to find out what is the best one can do with the current detector layout in terms of the above quantities, to recognize the problematic cases and to prepare the guidelines for a later attack with appropriate reconstruction algorithms.

In the ID part of this initial study only information from the Monte-Carlo generated events was used. Hits belonging to electron tracks were picked from the structures describing the detector and then fitted with the standard offline track fitting package. No pattern recognition is thus needed and so the results really show the optimal outcome of any algorithm searching for tracks in the ID.

As this was a combined ID/ECAL study the data-sets were analysed in three $|\eta|$ ranges: $[0, 0.6]$, $[0.6, 1.9]$ and $[1.9, 2.5]$. The first one corresponds to a pure barrel section of the detector with the least traversed material. The second one is a barrel to end-cap transition with some of the worst materialistic horrors as most of the barrel services enter the ID in this region. The last one is a pure forward tracker (see Fig:1.4 for a schematic view of the inner tracker).

Technical note: The 5 and 20 GeV e^- datasets used for this analysis were produced with DICE 97_6 simulation chain. This is the same ID layout as was used for the Physics TDR, but the ECAL reconstruction code is slightly outdated. In the detector simulation phase a 1 MeV cut was applied to the secondary tracks, which means that bremsstrahlung photons with a lower energy were not stored in the output structures. The simulations were carried out with a constant solenoidal magnetic field $B = 2\,\mathrm{T}$ in the ID volume.

3.1.1 Bremsstrahlung in the ATLAS detector

High–energy (above a critical energy) electrons predominantly lose energy in matter through bremsstrahlung. The characteristic amount of matter traversed is called a *radiation length* ($X_0[\,\mathrm{m}]$, usually expressed as $\rho X_0[\,\mathrm{g\,cm^{-2}}]$) and is defined as the mean distance over which the electron's energy is reduced by a factor of $1/e$. The main dependence of X_0 is on the atomic properties of the material. An approximate formula [19], accurate to better than 2.5% (5% for He), is:

$$\rho X_0 = \frac{714.4\ \mathrm{g\,cm^{-2}A}}{Z(Z+1)\ln(287/\sqrt{Z})}. \tag{3.1}$$

Consider again Fig:3.1: electrons on their way through the ID will have a rough ride before they make it to the ECAL. As bremsstrahlung is a pure QED process, given enough trials, anything can happen. But, how often? To answer this question we should study the energy distribution of the emitted photons. To overcome the immense amount of theoretical work on this topic, a brief survey of the problems encountered is made with references to the literature. In following discussion E denotes the initial energy of the electron and k the momentum of the emitted photon. The quantity $y = k/E$ denotes the fraction of energy carried away by the photon.

A first calculation of the bremsstrahlung process was made by Bethe and Heitler in 1934 [20]. For introductory purposes a slightly more modern (1954) review by Heitler is recommended [21]. The calculation of the differential cross-sections is followed by a discussion on the screening effect for high energies ($E \gg m_e$), which leads to a decrease in the cross-section. A technical review in a modern field theory language is given in [22]. Both references also discuss the cancellation of infrared divergences by including an amplitude for elastic scattering when evaluating the $k \to 0$ case.

The theory proposed by Landau and Pomeranchuk [23](calculation by Migdal [24]; theory addressed to as the *LPM effect*) goes one step further by considering the interference of scattering amplitudes from a larger area determined by the wavelength of a photon transferring momentum to the surrounding media ($\propto E^2/k$). The net effect is a significant suppression (order of 10% in 1 to 100GeV range) of the low k photon emission. Improved calculations were carried out by Baier and Katkov ([25], [26]) to better explain the results of a recent SLAC experiment [27].

A brief overview of bremsstrahlung properties can also be found in the Review of Particle Physics [19].

A good rule of thumb for the whole energy range of electron physics in ATLAS is still: $k d\sigma/dk \approx \text{const}$. Deviations of up to 20% are present in the IR region $k/E < 0.1$.

In ATLAS detector simulation, bremsstrahlung photons are simulated with the `GEANT3` detector description and simulation package [28]. `GEANT3` uses functions fitted to a calculated data to generate random variables in the Monte-Carlo process and takes into account the Migdal corrections (refer to the manual for details, sections PHYS340 and PHYS341). In the following, a brief review of the simulated bremsstrahlung photon properties is given. The angular distribution and the k–spectrum are presented.

A favourable property of bremsstrahlung at ultra relativistic energies is that all photons are emitted parallel to the electron momentum. The angular distribution falls off exponentially: $dP/d(\Delta\varphi) \propto e^{-f(E)\Delta\varphi}$. $f(1\,\mathrm{GeV}) \approx 500$ which is already a factor 10 below the angular resolution of the ECAL. $f(E)$ increases with energy; e.g: $f(10\,\mathrm{GeV}) \approx 2700$ and $f(50\,\mathrm{GeV}) \approx 4300$. In practice this means that a bremsstrahlung photon emission results in a decrease of the electron momentum without a change in the momentum direction.

As transverse energy is more relevant to electron reconstruction, the event samples were generated at fixed transverse momenta (p_T). This corresponds to generating an electron with a flat energy distribution in the range $E = p_T$ to $E = p_T \cosh(\eta_{\max} = 2.5)$. Extraction of a clear event sample with a well defined E is therefore not possible. Instead an energy weighted photon distribution of the first photon emitted is shown for several energy ranges in Fig:3.2.

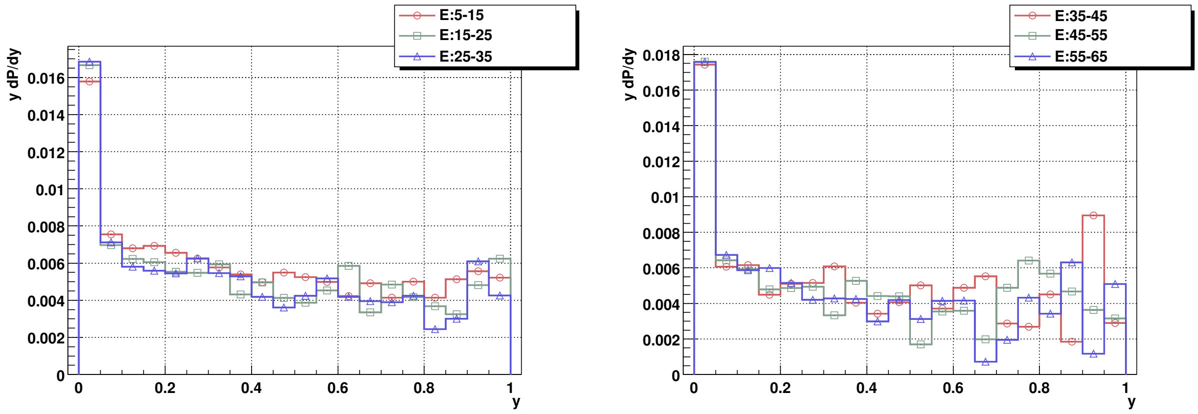

Figure 3.2: ydP/dy distributions of the first emitted photon for different energy ranges.

3.1.2 Electron energy losses in the ID

The first question asked is what fraction of $e^{\pm}$ lost more than a given percentage of their energy by a certain traversed distance in the ID. These losses are in direct correspondence with the systematic shift of a track's hits from its ideal (i.e., no bremsstrahlung) trajectory to its actual trajectory. Fig:3.3 shows the probability for an electron to lose 2%, 5%, 10%, 20% or 30% of its energy along its path for each of the three η regions. These losses are energy independent.

Here one should consider three points in more detail:

- 2% loss is to be compared to the statistical error from multiple scattering. After an electron loses more than 2% of its initial energy, systematic divergence from the fitted track can be observed.

- 10% loss is getting us into the tails of the calorimeter E_T measurement. These events should not be used for the ECAL calibration.

- 30% loss approximately corresponds to the $0.7 \leq E_T/p_T \leq 1.3$ cut used in the ID TDR for electron identification. In principle this cut should serve as a discriminator against the background while allowing for as high identification efficiency as possible. Often the choice between the two modes is specific to the analysis being performed.

  While this selects good electron candidates it also decreases the electron identification efficiency.

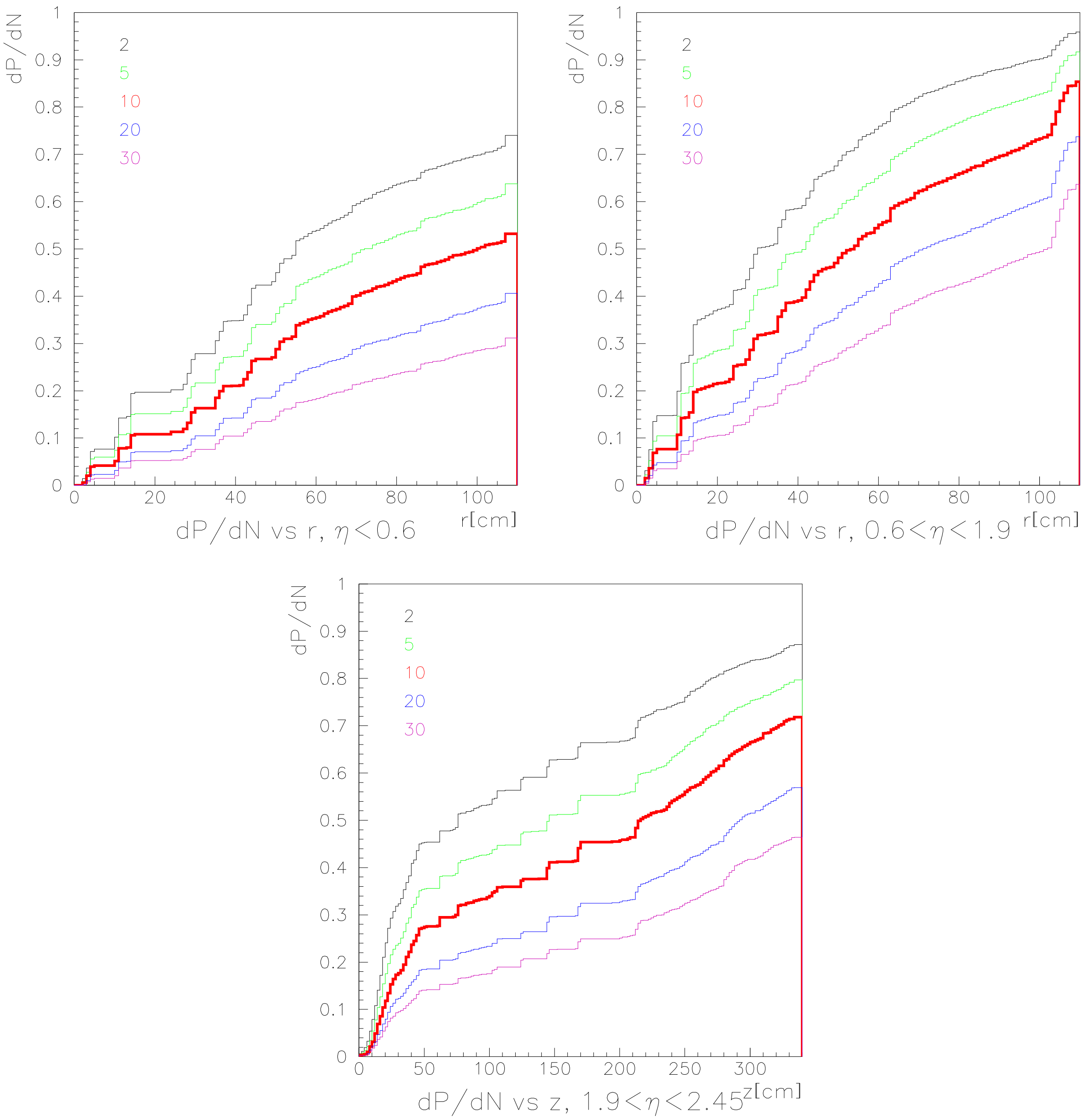

Figure 3.3: Fractions of electrons that lost more than certain percentage of their energy as a function of the distance traveled. Different colors correspond to the threshold of a different fractional loss. Each plot depicts one $|\eta|$ region.

Our goal, set at this point, was to improve the reconstruction of electrons losing more than 10% of their energy by the outer radius of the SCT. This would allow a harder cut on E_T/p_T and to better discriminate against the background as well as improve the identification efficiency. Tab:3.1 shows what fraction of the overall electron population are being addressed.

We need at least three points for a p_T measurement which corresponds to a track reconstruction in only the pixel detectors. Therefore the electrons losing more than 10% of their energy by the end of the pixels represent the irreducible background for which ID stand-alone reconstruction cannot make a good p_T measurement. All SCT measurements of these $e^{\pm}$ are plagued by a systematic shift.

η bins	$0-0.6$	$0.6-1.9$	$1.9-2.45$	weighted sum, all η
pixels	0.11	≈ 0.22	0.35	0.22
SCT	0.32	≈ 0.58	0.45	0.49
TRT	0.52	≈ 0.75	0.70	0.68

Table 3.1: The fraction of $e^{\pm}$ that have lost more than 10% of their energy by the end of each ID sub-detector. The three $|\eta|$ regions are shown together with the weighted average over the full ID η-coverage. The values in the table include the cases where the bremsstrahlung occurs close to the end of the sub-detector in question and are therefore a pessimistic estimation of the degradation of the reconstructed momentum.

In principle a vertex constrained fit could be used to improve the resolution. But this solution is not generally applicable because of the electron signal from displaced vertices such as B decays or early γ conversions (giving rise to over–corrected p_T). The application of this procedure is therefore limited to the reconstruction of narrow resonances selected according to an invariant mass cut.

3.1.3 Distributions of fitted p_T

The second question is how do the p_T distributions vary when we go along the track and keep adding in new measurements? We start with a pixel-only fit and then include SCT measurements, one layer (two measurements) at a time. To make the situation clearer, four samples were chosen according to the `GEANT3` tracking information:

- △ **Less** than 10% loss by the end of the SCT. This is the purest sample where we expect all subsequent measurements to improve the reconstructed p_T.

- ● All events; this provides a view of the overall situation and enables one to see individual influences on the big picture.

- ☆ **More** than 10% loss by the end of the pixels. These are catastrophic events where the tracker cannot make a good p_T measurement. By adding in new measurements the resolution should even deteriorate.

- ◊ **More** than 10% loss by the end of the SCT, excluding ☆. A good p_T measurement should be possible, but it is expected to give a poorer resolution through being too greedy in number of measurements.

Fig:3.4 shows the raw distributions for the best and the worst sample. The △ sample distribution becomes more Gaussian-like when adding in new measurements, while the ☆ one is running away from it by pulling in a longish low-p_T tail. A statistical view of the p_T distributions is shown in Fig:3.5. The mean values are systematically decreasing, going further and further away from the *true* value. The rms is around 0.3 for a pixel–only measurement, which is easily understood as the pixel measurements are lined up close together in r/z. The addition of a single SCT layer basically stabilizes the rms at a flat line.

We can also look at the problem from another angle and ask: What fraction of the reconstructed $e^{\pm}$ is outside a $0.9 \leq \frac{p_T}{p_T^{\text{true}}} \leq 1.1$ selection? Fig:3.6 shows the results. There are two major points. Firstly, even in the best case (less than 10% bremsstrahlung), insisting

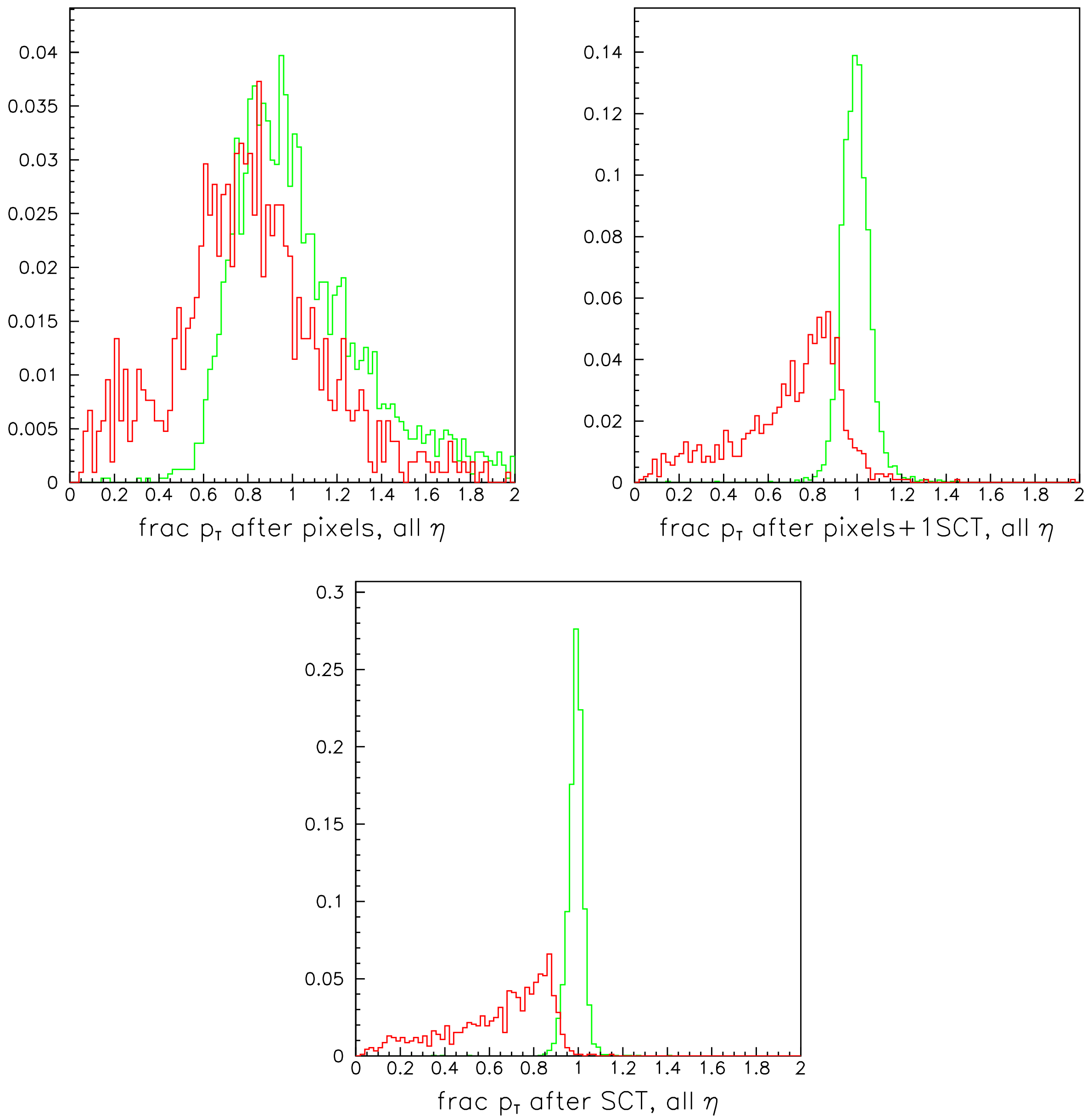

Figure 3.4: Raw p_T/p_T^{true} distributions for cases when 3, 4 or 7 measurements are included in the fit (see subtitles of plots). The red histogram in each plot corresponds to the ☆ sample and the green one to the △ one. Note that $1/p_T$ has a Gaussian distribution; p_T is shown as it better depicts the bremsstrahlung-tail.

on a full track length for the p_T measurement is futile. Secondly, reading from the minima of ● points, one finds the sad reality of electron reconstruction in ATLAS: bremsstrahlung recovery by cutting back on the number of measurements (or a two curvature fit, which allows for use of the full PR & TR info) will yield at best 15, 25, 35% of electrons outside the 10% limit (per η region). Still, one can compare this to an $\sim 50\%$ inefficiency obtained by requiring a full length track without any bremsstrahlung recovery (see Tab:3.1).

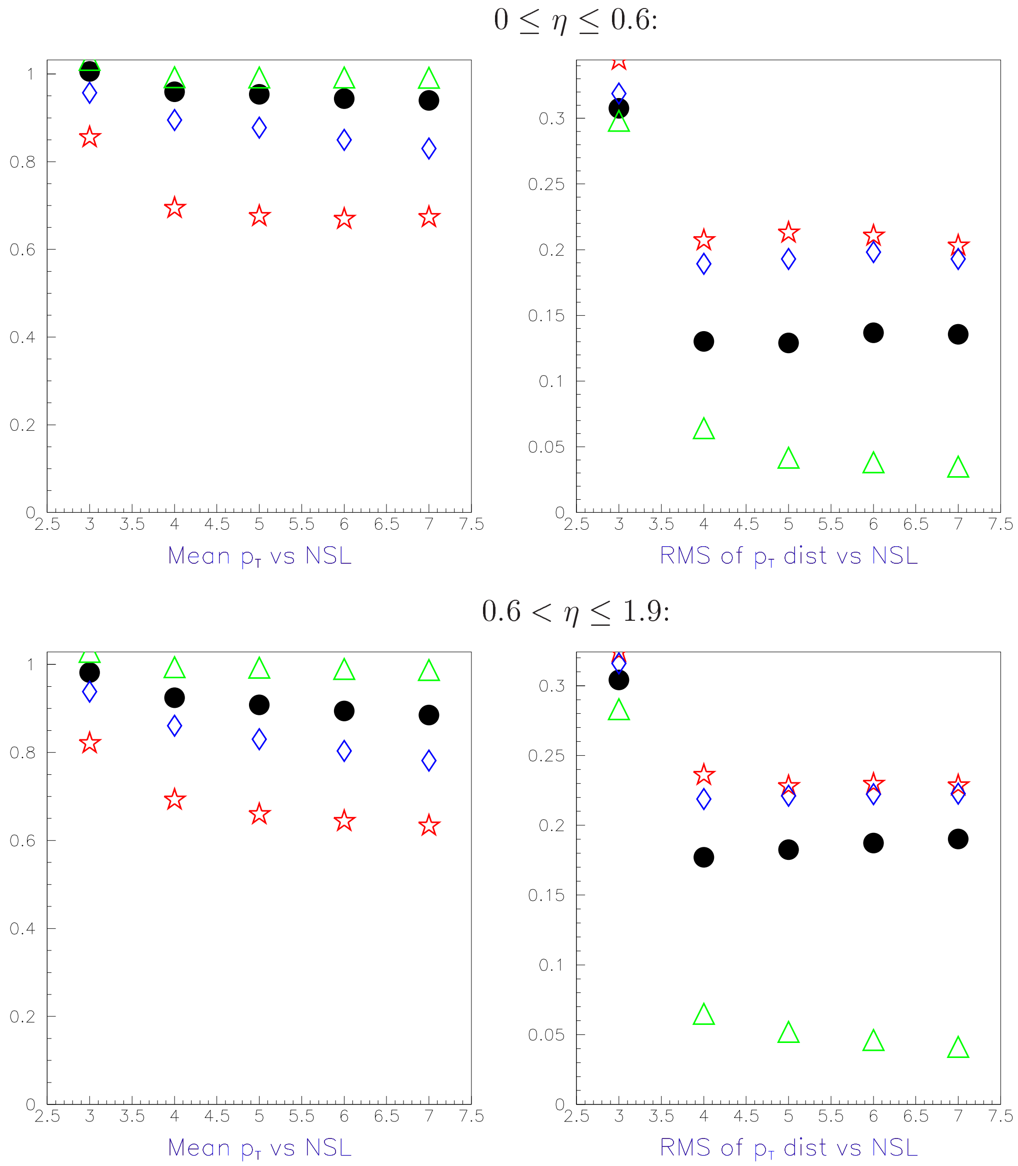

Figure 3.5: Mean & rms of the p_T/p_T^{true} distributions versus the number of layers (NSL) used in the fit. The barrel and transition regions are shown.

3.1.4 E_T/p_T matching

As already mentioned in the introduction, matching of the energy measured by the calorimeter to the momentum of the track reconstructed in the tracker is one of the primary means for electron identification. This and the following section address this topic.

Fig:3.7 shows the E_T/p_T match and Tab:3.2 gives the fraction of events that satisfy different cuts on this quantity. The p_T was chosen from the fit corresponding to the number of measurements giving the minimum fraction outside the 10% cut (4 for the 2$^{\text{nd}}$ bin; 5 for the other two), i.e., the fit with the best possible ID performance. The relevant observation is that blindly accepting a single value for E_T/p_T cut will reduce the electron identification efficiency at lower energies.

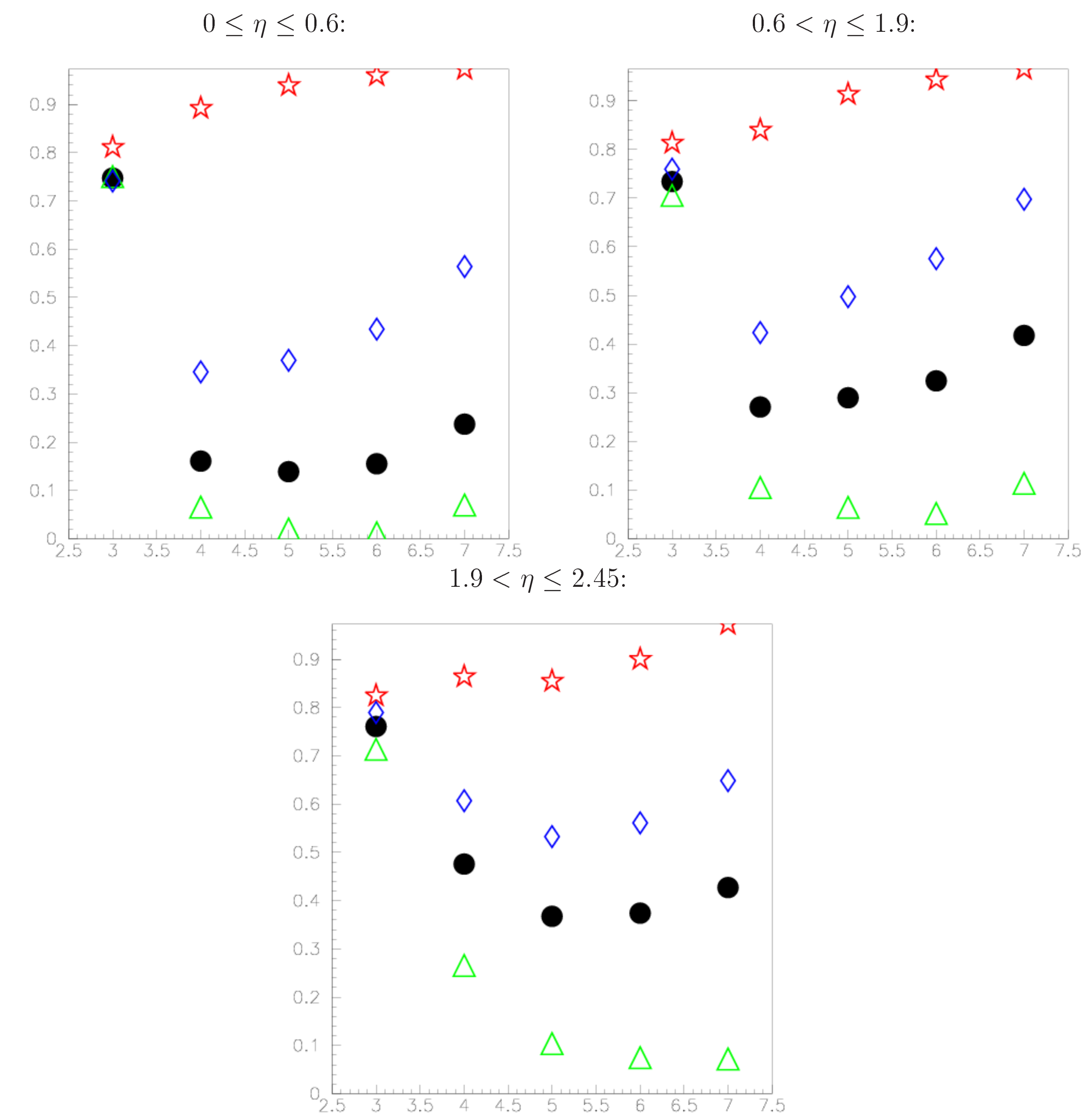

Figure 3.6: Fractions of electrons out of a 10% selection on p_T/p_T^{true} as a function of number of crossed layers. Fractions are shown for the three η regions and for four event samples.

frac within	20 GeV				5 GeV			
E_T/p_T cut	△	●	☆	◊	△	●	☆	◊
0.7-1.3	1.00	0.92	0.60	0.84	0.99	0.94	0.79	0.88
0.8-1.2	0.99	0.88	0.43	0.76	0.98	0.89	0.66	0.77
0.9-1.1	0.93	0.76	0.17	0.57	0.88	0.73	0.41	0.55

Table 3.2: Fractions of events that satisfy different E_T/p_T cuts, integrated over all η.

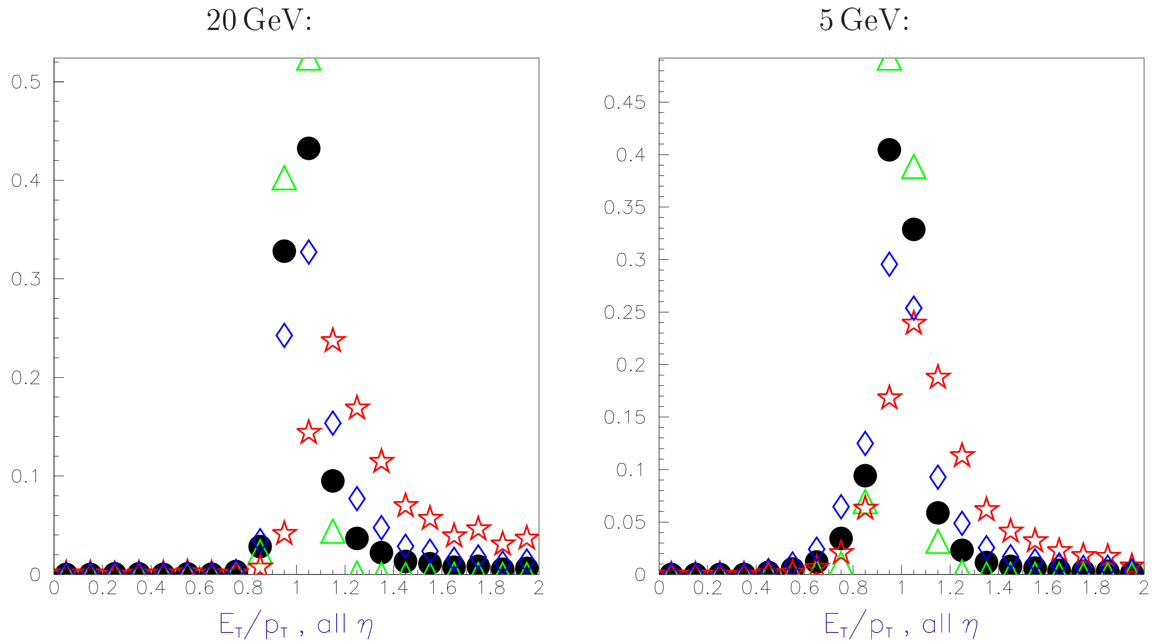

Figure 3.7: E_T/p_T distributions for four event samples over all η.

3.1.5 ECAL reconstruction

As the ID will not be used in the level 1 trigger(1.4.2), the first beast prowling for unfortunate electrons is the ECAL reconstruction inefficiency. To understand some of the peculiarities that we will meet in further discussion, a short description of the clustering algorithm is presented.

The ECAL clustering algorithm begins by collecting the contributions from all samplings (without the crack scintillators!) in a combined matrix with a grid size $(\Delta\eta \times \Delta\varphi) = (0.025 \times 0.025)$ corresponding to the cell size of the second sampling. Calibration corrections are applied in the process. The cluster search uses a sliding window algorithm with an adjustable window size. The algorithm centres the window such that the sum of the contained energy is maximized. For electrons a window size of 3×7 ($\eta \times \varphi$, in grid units) gives good results as it allows most of the bremsstrahlung photons to be included in the same cluster as the electron. A threshold of 1.1 GeV (clustering cut) is usually used to minimize the effects of electronic noise and contributions from minimum bias pile-up.

HCAL clustering uses the same philosophy, only the grid segmentation is four times coarser. The matrix is filled with the sum of the transverse energies in the EM (including the scintillator!) and hadronic sections, smeared according to the real cell size. The search for jet candidates uses a 3×3 window while kinematic variables (positions and spreads) are calculated using a 9×9 window centered around the found maximum. The typical clustering cut is 2 GeV.

As we are interested in performance of the calorimeter down to the lowest reasonable limit of $E_T \sim 1.5$ GeV, we used somewhat lower clustering cuts for single particle analyses: a threshold of 1 GeV was set on the E_T contained in an EM cluster for $E_T^{\text{true}} > 10$ GeV and 0.7 GeV for $E_T \leq 5$ GeV. Still, there are two reasons causing some electrons with $p_T > 1$ GeV to fail this cut:

E_T		1.5	2	3	5
$E_T^{\rm cut} = 0.7\,\rm GeV$	all	70.9	89.1	97.1	99.3
	transition	52.6	80.4	94.5	98.6
$E_T^{\rm cut} = 1.0\,\rm GeV$	all	41.9	74.6	94.4	98.6
	transition	19.2	58.0	89.5	97.3

Table 3.3: Efficiency of the EM calorimeter at low transverse energies for clustering cut set to $E_T = 0.7\,\rm GeV$ and $1\,\rm GeV$. Values are quoted for all events integrated over η and for the transition region, where the efficiencies are at their worst.

	20 GeV		5 GeV	
ΔE_T	△	☆	△	☆
mean	0.01	0.03	0.07	0.17
rms	0.05	0.06	0.12	0.15

	20 GeV		5 GeV	
$\Delta R/Z$	△	☆	△	☆
mean	0.01	0.01	0.01	0.04
rms	0.25	0.26	0.56	0.60

	20 GeV		5 GeV	
$R\Delta\varphi$	△	☆	△	☆
mean	0.01	0.24	0.14	-0.47
rms	0.77	1.15	2.45	3.75

Table 3.4: Mean values and rms's of the residuals of calorimeter measurements for the △and ☆event samples (representing 51% and 22% of the event sample respectively).

1. For a very low p_T (up to $3\,\rm GeV$) the bremsstrahlung can split the energy between two distinct clusters causing both of them to fail the E_T cut. This is most likely to happen in the regions with a large amount of material in front of the ECAL.

2. There is a crack at the join of the barrel and end-cap module ($|\eta| = 1.5$). An electron with p_T lower than $\sim 10\,\rm GeV$ can sneak through this crack with a minimal energy deposition and therefore miss the E_T threshold. Also, as the EM cluster searching algorithm does not include the crack scintillator measurement, some clusters can be lost even if a measurement has been made.

Tab:3.3 gives the ECAL reconstruction efficiencies at low energies for the two choices of the clustering cut. For 10 GeV and above the reconstruction is fully efficient.

E_T, η and $R\varphi$ matching

For electron identification the EM cluster is required to match the track in the ID. This section compares the ECAL measurements with the quantities projected from the true parameters at the vertex. Fig:3.8 shows the residual distributions and Tab:3.4 gives their statistical description in terms of a mean value and rms for the best and worst case (as seen by the amount of brem–losses).

The following conclusions can be made:

- In ΔE_T the bremsstrahlung effects can be seen as a missing energy. Usually this means that the electron didn't make it into the 3×7 window used for clustering.

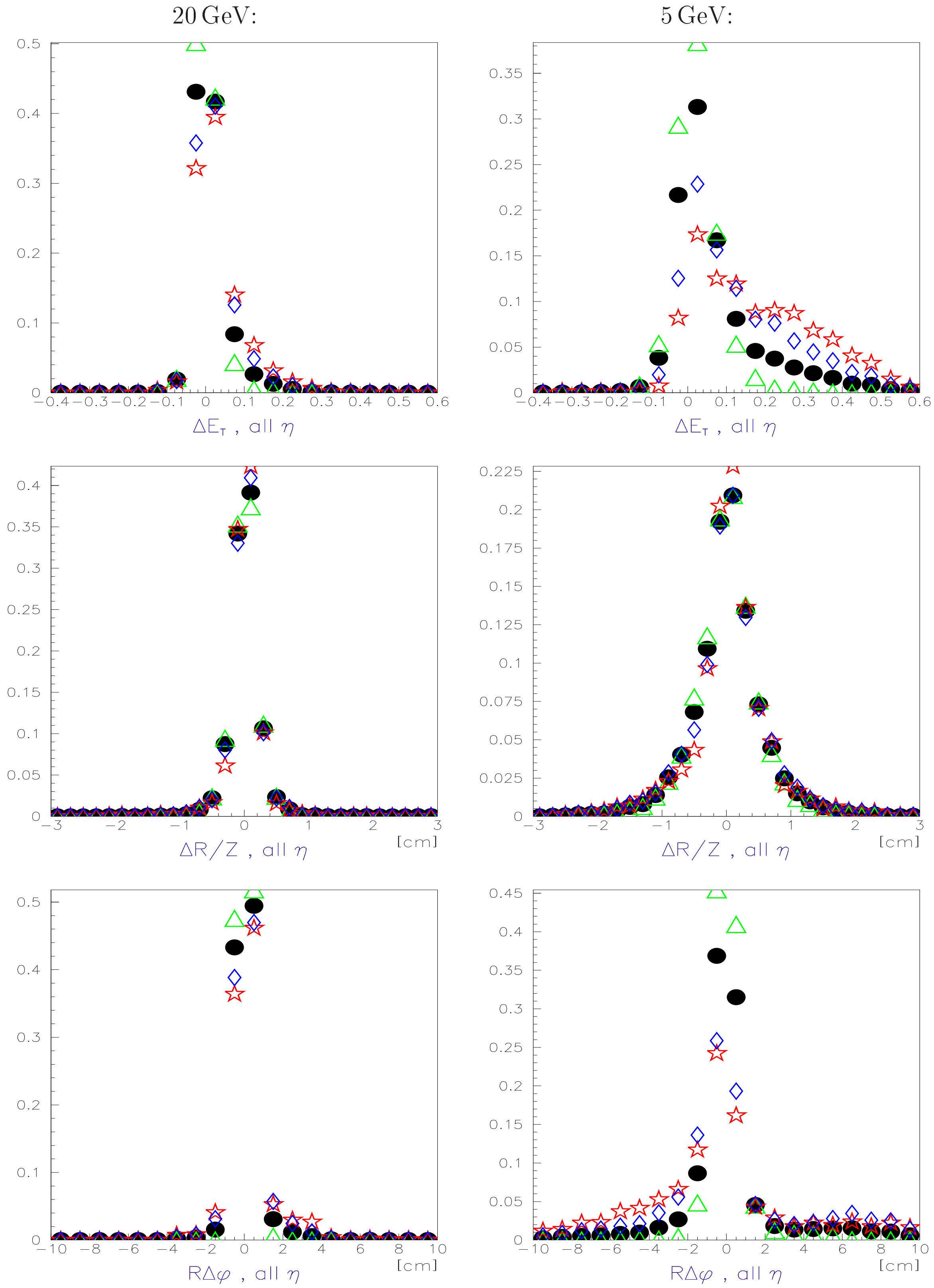

Figure 3.8: Residuals of the calorimeter energy and position measurements (expressed as difference $\frac{\text{true}-\text{reconstructed}}{\text{true}}$) for $E_T = 20\,\text{GeV}$ (left) and $5\,\text{GeV}$ (right). ΔR is used for the end-cap and ΔZ for barrel measurement.

- $R\Delta\varphi$ shows two effects: there can be a γ (a small bump on the positive side of the residual distribution) or an electron (longish tail on the negative side) falling out of the ECAL window.

- No bremsstrahlung effects can be observed in the longitudinal ($\Delta R/Z$) measurement.

This leads us to the conclusion: provided the energy is contained in the calorimeter window its position measurement is independent of bremsstrahlung. In the hard bremsstrahlung case, one can still use R/Z (or η) matching for $e^{\pm}$ confirmation.

To further investigate the correlation between ΔE_T and $R\Delta\varphi$, consider Fig:3.9. The systematic bumps from early hard brems that miss the 3×7 window can be seen for the 5 GeV sample. At 20 GeV one is basically saved from this kind of magnetic field induced loss.

20 GeV: 5 GeV:

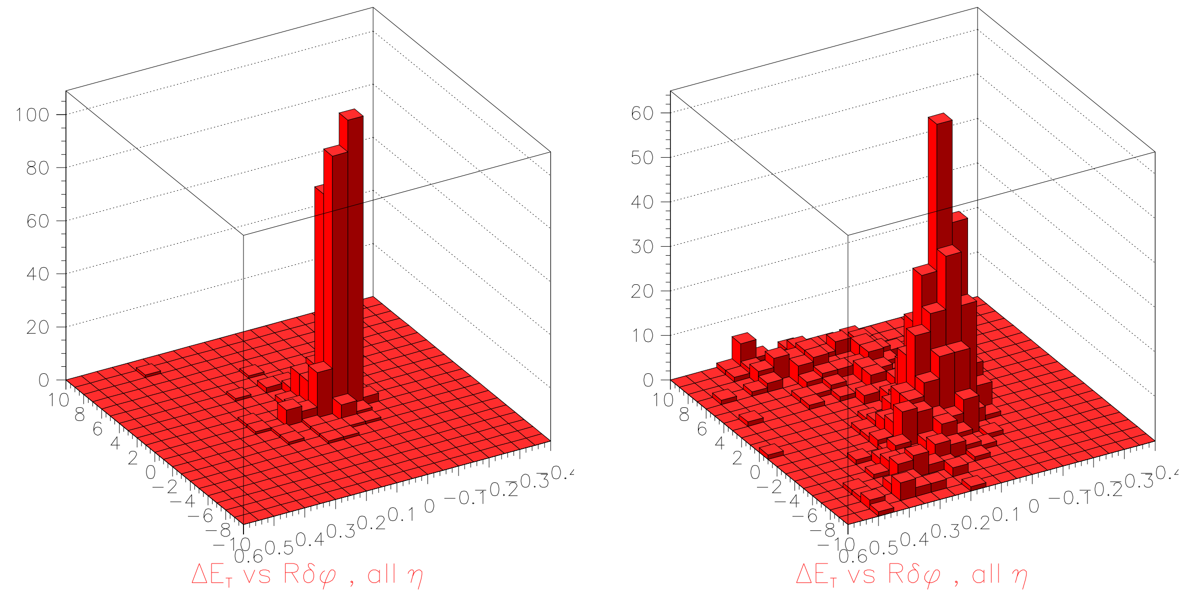

Figure 3.9: Distribution of the ☆ event sample over the $\Delta E_T(\swarrow) \times R\Delta\varphi(\nwarrow)$ plane.

The $E(\varphi)$ distribution and multiple EM clusters

As the electron and the emitted photon are separated by the magnetic field, one would expect this separation to reflect in the spread of the energy distribution in the EM cluster. At low energies (up to 10 GeV) this effect can indeed be observed but it is not very pronounced. A brief analysis showed that the ID measurements allow for a better bremsstrahlung tagging, thus the question will be revisited only when the ID pattern recognition is 'used up'.

Another problem occurs when the electron/photon separation produces two EM clusters. Due to the algorithm used in cluster reconstruction, these two clusters can partially overlap (see [29] for details of the algorithm). A simple method of resolving this ambiguity was developed and will also be discussed later.

3.1.6 Is a first order bremsstrahlung treatment sufficient?

Basically the question is: Is a bremsstrahlung treatment to the first order sufficient or is there a relevant fraction of events where two (or more) photons take away a significant amount of the energy? Higher order effects can be very tricky to reconstruct properly as each separate bremsstrahlung produces a kink on the track and introduces new unknowns to the pattern recognition process.

We proceed with a short overview of the properties of the hardest (primary) and the second hardest (secondary) emitted photon. First consider the distribution of the number of emitted photons (above the 1 MeVcut-off) versus η (Fig:3.10). As expected, it follows closely the material distribution. By taking into account the way the simulation of the bremsstrahlung is performed and the E_γ distribution (see Sec:3.1.1), we expect a first order treatment to be justifiable in the barrel and to some extent also in the end-cap region.

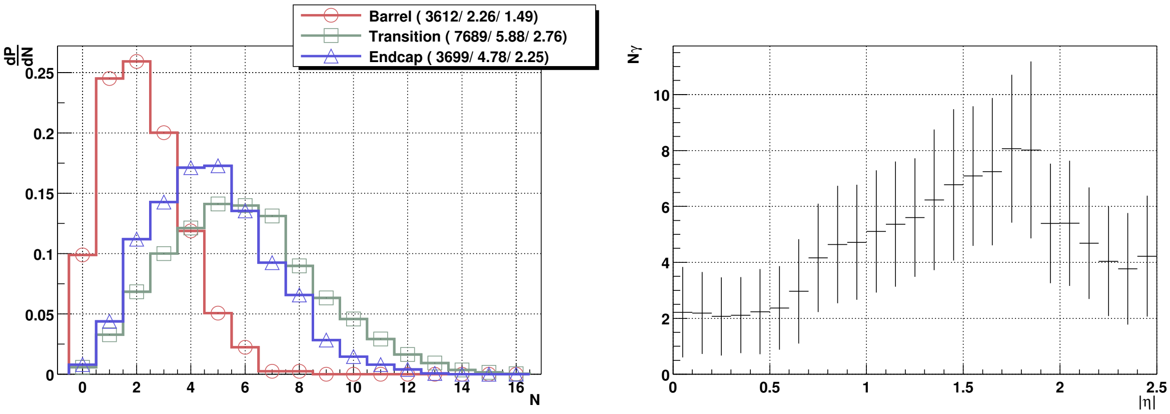

Figure 3.10: Left: The distribution of the number of emitted photons (above the 1 MeVcut-off) for the three η regions. Right: The mean number of photons versus $|\eta|$; the error bars represent the rms.

To get a qualitative measure of the effect the cumulative distribution of the probability for the photon in question to take away a certain fraction of all the emitted energy was plotted. (Fig:3.11). As these plots are a bit hard to read, Tab:3.5 summarizes the results. The conclusion is somewhat sad: a second order treatment is necessary in about half of the cases. The numbers are a bit overestimated as for two close photon emissions the pattern recognition can safely treat them as a single one. Also ... a bremsstrahlung close to the end of the TRT is harmless in view of the silicon oriented reconstruction. For completeness, the fractional amounts of bremsstrahlung loss by the end of the ID's sub-detectors are also given (Fig:3.12). This information can be combined with the above fractions to pinpoint the different cases for pattern recognition.

3.1.7 Expected cases

All these things considered, we can come up with different scenarios and probabilities for each of them to occur. We present three different methods of inspection. The first one is a cumulative tree with branchings occurring at the end of each of the sub-detectors (see Tab:3.6). This representation gives one a good feeling for the beginning of the track and where in the detector things start to go wrong.

	% bremmed energy	Barrel	Transition	Endcap
Primary	≥ 90	0.26	0.12	0.21
	≥ 80	0.47	0.27	0.38
	≥ 70	0.62	0.42	0.53
Primary + Secondary	≥ 90	0.69	0.40	0.56
	≥ 80	0.87	0.67	0.79
	≥ 70	0.95	0.84	0.91

Table 3.5: The fraction of events where the primary (primary + secondary) photon took more than 90,80,70% of all the energy radiated.

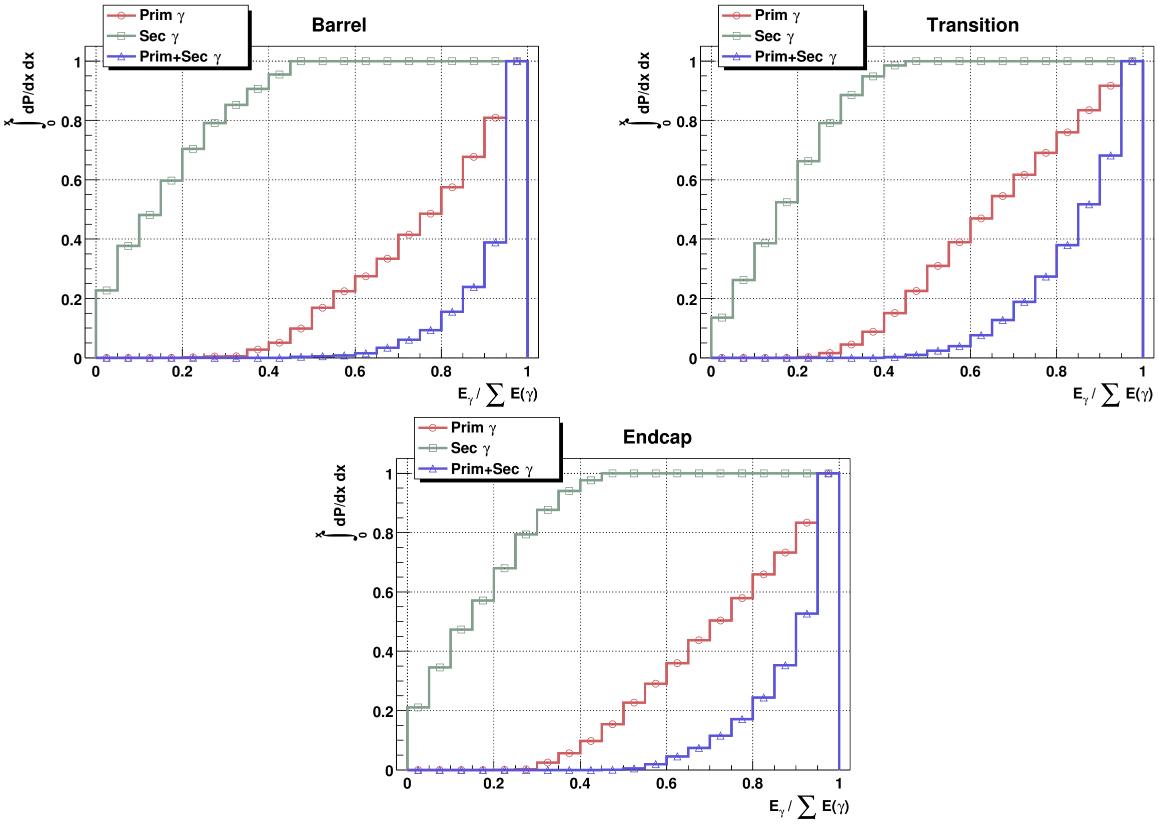

Figure 3.11: Cumulative probability distributions for the hardest(`Prim`) and second hardest(`Sec`) bremsstrahlung photon as well as their sum to take more then certain fraction of all emitted energy. The three η regions are separated.

The second representation is a bit more cumbersome as it treats each of the sub-detectors separately. We separate three cases for each sub-detector:

S (small) less than 2% loss in the sub-detector. No special treatment is necessary.

M (medium) loss between 2% and 10%. Some of the effect can be swept under the rug as a multiple scattering tail or by a degradation of the fit parameters. These events are basically hard to spot and reconstruct properly.

L (large) above 10% loss. The kink is more evident and can be found provided that enough measurements exist on both sides.

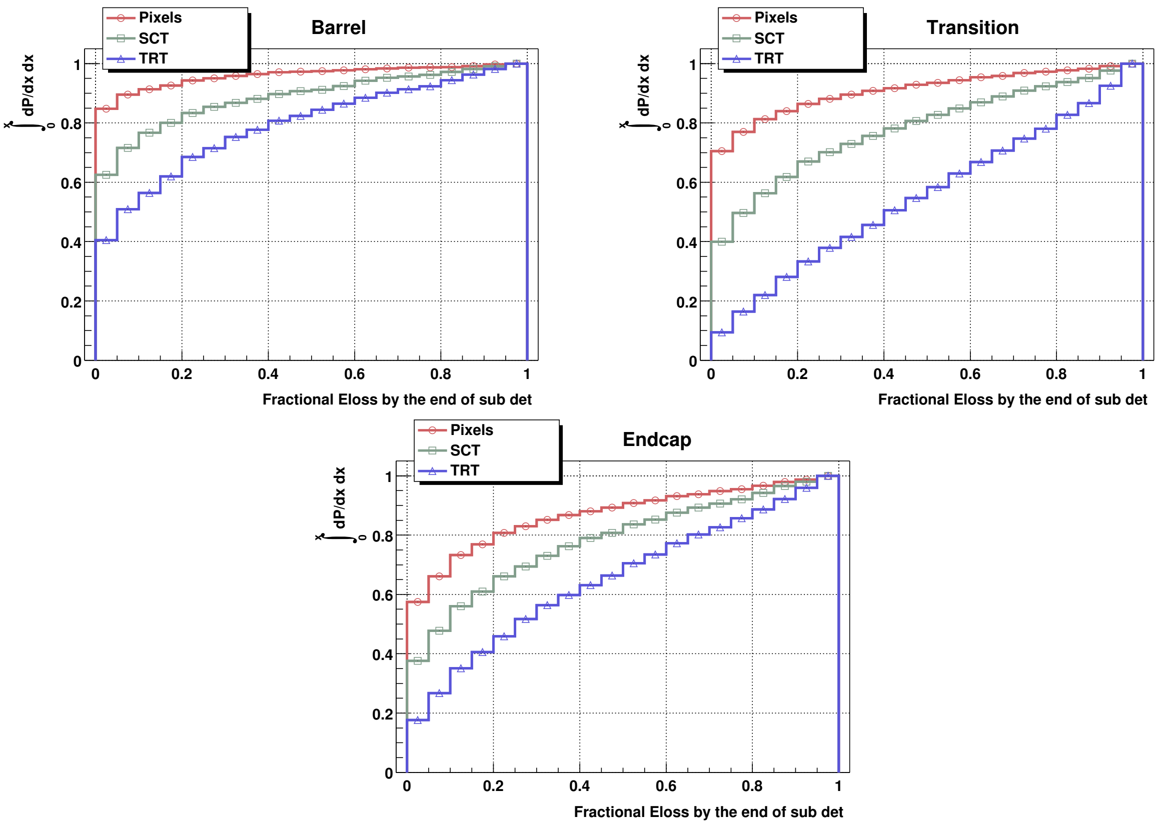

Figure 3.12: Cumulative probability distributions for an electron to lose certain fraction of all energy carried away by the bremsstrahlung by the end of the three sub-detectors.

This gives the 3^3 different cases presented in Tab:3.7. Here one can directly recognize different pattern recognition scenarios.

y_{Pix}	y_{SCT}	y_{TRT}	Barrel	Transition	Endcap
< 0.1	< 0.1	< 0.1	0.509	0.164	0.267
		> 0.1	0.207	0.332	0.210
	> 0.1	< 0.2	0.037	0.022	0.042
		> 0.2	0.143	0.251	0.142
> 0.1	< 0.2	< 0.2	0.012	0.011	0.035
		> 0.2	0.007	0.028	0.035
	> 0.2	< 0.3	0.017	0.009	0.036
		> 0.3	0.070	0.183	0.233

Table 3.6: Expected bremsstrahlung cases in electron reconstruction: cumulative view over the sub-detectors.

The third method is in fact a merge of the above two with an emphasis on silicon based reconstruction. The TRT is considered only as a bridge between the silicon tracker and the ECAL. By comparing the electron track to a non-electron track from the reconstruction's point of view we find the following bremsstrahlung scenarios:

Pix	SCT	TRT	Barrel	Transition	End-cap
S	S	S	0.304	0.054	0.119
S	S	M	0.090	0.063	0.052
S	S	L	0.141	0.190	0.105
S	M	S	0.063	0.021	0.029
S	M	M	0.020	0.021	0.011
S	M	L	0.033	0.073	0.026
S	L	S	0.089	0.050	0.063
S	L	M	0.027	0.049	0.024
S	L	L	0.039	0.101	0.026
Pix = S sum:			0.806	0.622	0.455
M	S	S	0.040	0.014	0.050
M	S	M	0.009	0.017	0.024
M	S	L	0.012	0.036	0.051
M	M	S	0.005	0.005	0.014
M	M	M	0.002	0.006	0.008
M	M	L	0.006	0.016	0.008
M	L	S	0.012	0.010	0.024
M	L	M	0.002	0.014	0.013
M	L	L	0.002	0.030	0.014
Pix = M sum:			0.090	0.148	0.206
L	S	S	0.043	0.033	0.127
L	S	M	0.016	0.031	0.042
L	S	L	0.007	0.059	0.062
L	M	S	0.012	0.010	0.028
L	M	M	0.002	0.015	0.010
L	M	L	0.002	0.021	0.008
L	L	S	0.016	0.021	0.033
L	L	M	0.002	0.019	0.014
L	L	L	0.003	0.021	0.014
Pix = L sum:			0.105	0.230	0.339

Table 3.7: Expected bremsstrahlung cases in the electron reconstruction: detailed view. See text for explanation of symbols.

1. **Negligible amount of bremsstrahlung (55% of events):** below 10% energy loss by the end of the SCT. This events can be handled with the usual fitting procedure.

2. **Single measurable bremsstrahlung photon emission (12%):** above 10% energy loss by the end of the SCT. The primary photon originates from the SCT and takes more than 80% of all the emitted energy. ID bremsstrahlung recovery can be applied.

3. **Early hard bremsstrahlung photon emission (10%):** as above with the hardest brem within the pixels. Can be reconstructed with a poorer p_T resolution. It remains to be seen how well these events can be tagged.

Case	Barrel	Transition	End-cap
1	0.716	0.496	0.477
2	0.122	0.122	0.116
3	0.066	0.080	0.190
4	0.096	0.302	0.217

Table 3.8: The expected bremsstrahlung cases encountered during electron reconstruction according to a silicon oriented classification. The four cases are defined in the text.

4. **Two (or more) hard bremsstrahlung photon emissions (23%)**, early ones not excluded. Recuperation of these events is questionable as it depends on several factors. Further investigation in the reconstruction environment is necessary to determine the possible outcomes.

The numbers in brackets give probabilities over the whole η coverage. The fractions for each of the sub-regions are given in Tab:3.8. The 80% cut on brem–hardness is somewhat arbitrary. By decreasing it to 70%, 5% of the events are 'transferred' from case 4 to cases 2 and 3.

3.2 Electron reconstruction algorithm

In the framework of ATLAS software three track reconstruction packages are being maintained:

- `iPatRec` is a pattern recognition package with a combinatorial search starting in the silicon layers. It is optimised to work in roads defined by the seeds from the calorimetry or muon system to avoid unnecessary processing in on-line and high-luminosity environments.

- `PIXLRec` puts its emphasis on exploiting the fine granularity of the pixel detector. Its aim is to test an alternate algorithm for track-finding, and thus obtain a more reliable understanding of the Inner Detector performance, especially in the b-tagging area. It is not meant to be a professional package and is not optimised for speed.

- `XKalman` starts its pattern recognition in the TRT using a histogramming method. Tracks are then projected into the precision layers using the Kalman filter–smoother formalism.

In short: `iPatRec` and `XKalman` are two track finding packages with very different basic algorithms. In an experiment of ATLAS's size it is vital to have several independent programs to allow for cross-checks regarding the reconstruction efficiency and execution speed.

All the work presented here was done in the framework of `iPatRec`. As `XKalman` already has a special electron treatment built into its guts, most of the algorithms developed can be seen as an extension of `iPatRec`, giving it electron identification and bremsstrahlung recuperation abilities. Historically, `iPatRec` had the option of a bremsstrahlung fit, which allowed for a kink on the track. Following the analysis presented in the previous section it was decided that this was inadequate as a first order treatment of bremsstrahlung is only appropriate for a limited fraction of events.

The fact that the developed algorithm is in a way an extension of `iPatRec` led to another design decision. As `XKalman` is seen more like a TRT based algorithm and `iPatRec` more as a SCT based algorithm, the TRT was intentionally not taken into account with its full design capacity. The TRT's tracking information, forming a base of the `XKalman`'s track searching logic, was only considered as a bridge between the silicon and the EM calorimeter and the TR information was extracted to play its part in the e/π separation. More emphasis was put on the EM calorimeter and its matching to the silicon reconstructed tracks. This introduces a higher level of redundancy in the electron identification should it turn out that the TRT does not function as well as anticipated.

As the understanding of the algorithm requires some references to the world surrounding it, a brief description of the reconstruction environment is made first. The algorithm itself is then explained together with its inner workings, and the rationale behind the imposed logic. But first let us briefly review the goals of the algorithm.

1. **Electron identification** is a prerequisite for the algorithm. The problematic aspects of identification are the separation of electrons from photons and pions, as well as identification in jets where the ECAL is polluted with depositions from hadrons.

2. **Bremsstrahlung tagging** is important to separate the wheat from the weeds. It is essentially linked to the electron identification because bremsstrahlung can lead to a degradation of the quantities used for identification.

3. **An improvement of p_T resolution** is important especially at energies below 20 GeV where the tracker precision is better than that of ECAL. As a kind of feedback it enables a better ECAL calibration.

4. **Improvement of perigee parameters** allows for smaller errors when fitting two electrons back to their common vertex. The impact parameter resolution is closely related to the p_T resolution.

Disclaimer: It has already been shown in Sec:3.1.7 that only about 50% of electrons can be reconstructed in their full vigor. The others are of a more or less questionable nature. A lot of effort has been put in being honest about what happened to the particular electron. Also no miracles were attempted as they turn out to cause more harm than good. In the case of an early bremsstrahlung photon emission no correction is applied to the track parameters to make the track fit the EM cluster better. Rather the best measurement available from the ID is chosen and the electron is tagged as a candidate for the occurrence of a disastrous bremsstrahlung. The dubious cases are left to a later stage of the analysis to decide how to deal with them. Thus a good systematic error assessment can be made and/or the best statistics out of the available event sample can be collected.

At this point it is appropriate to give a proper name to the electron reconstruction and identification package developed. In a way it has to be more than a mere algorithm as it has to talk to the outside world and be aware of special conditions that have nothing to do with anything else but the ATLAS detector.

`ieElRec`, Ego te baptizo in nomine Patris, et Filii, et Spiritus Sancti.

3.2.1 `ieElRec`'s habitat

It is not my intention to go into the depths of the geometry description of the detector, event structure and low–level detector reconstruction. Also I will not discuss how this information is carried over into the reconstruction environment and how it's kept there. Mentioning this topic and remarking that it is far from being trivial is sufficient for my purposes.

In essence, the whole business of pattern recognition is in transforming raw measured (or simulated) data into physical quantities. This is done in several stages:

1. In the ID the measurements are 'collected' into tracks and in the calorimeters they are grouped into clusters. Clusters are subjected to calibration and algorithmic corrections which render low level calorimeter measurements mostly useless for further analysis.

2. Special identification packages are run on top of that information. Results from them can be identified particles, reconstructed short–lived particles (decaying near the collision point) or just improvements to the measurements of certain quantities.

3. Later all this information is used in an analysis program serving some more physical goal, e.g., the spectroscopy of a new particle or the study of a special decay channel.

In terms of this enumeration `ieElRec` belongs to the 2$^{\text{nd}}$ step. Taking the tracks and EM clusters from the 1$^{\text{st}}$ step (`iPatRec` and ECAL reconstruction) it identifies electrons, determines what and where went wrong (i.e., bremsstrahlung identification), corrects what can be corrected (i.e., bremsstrahlung recuperation) and provides information used for background rejection.

Basics of `iPatRec`

As already mentioned above, `iPatRec` is optimised to run in roads defined by the calorimetry or muon system (with the general term `seed` used to describe any of the above). A road is a region of the detector obtained by projecting the η and φ coordinates of the seed to the vertex region. The algorithm can be made to work over all coverage of the ID by decomposing it into several roads with a small overlap in η and φ.

After initialization of the road `iPatRec` gathers all silicon hits within the road. The SCT hits from the same module are joined into *space-points* which are used in the search initiation phase only. The pixel hits form space-points directly. Then the combinatorial searches start. The result of the search is of course a list of tracks. Three types of tracks can make it to this final list:

- **Primary tracks** are full length tracks from the vertex region to the outer regions of the TRT.
- **Truncated tracks** have an association to the vertex region but fail the outward extrapolation.
- **Secondary tracks** fail the vertex association but succeed in outward extrapolation to at least some part of the TRT.

All of them are subjected to a quality control which assures a good efficiency and a low fake rate. The standard sample used for checking that the tracks have good quality are b-jet events with high luminosity pile-up which gives the highest detector occupancies expected in ATLAS.

A brief and crude description of the combinatorial search is given here as it is needed for an understanding of the track types produced by `iPatRec` and used by the electron reconstruction algorithm.

All in all there are ten combinatorial searches performed per road. Each of them is seeded from the combinatorials constructed from the space-points coming from a pair of layers designated as ‘outer’ and ‘inner’ layers. The choice of these search initiating layers is optimised with respect to execution speed and to give sufficient robustness against a realistic level of detector inefficiencies. Special patterns, targeted at short tracks (truncated and secondary) visible only in the inner or outer layers of the tracker are also included. For example the first search is performed by considering the combinatorials from the outermost and second SCT layer. The following is a more algorithmic transcription of the `iPatRec`’s search logic.

1. The first loop is made over all ‘outer’ points. For each of the outer points a reference to the best track is kept through the inner loops for each of the three kinds of tracks mentioned above. These are not their exact counterparts but rather candidates that are waiting to be promoted to this status. There is an implicit assumption that hits are unique – can only belong to one track – in the ‘outer’ layer.

2. The second loop is made over all ‘inner’ points. For each of the combinatorial *candidates* a loop is made over all points in ‘check’ layers until a first point compatible with the hypothesis of the track originating from the interaction point is found. Otherwise this combination is discarded.

3. A two point track is first constructed from the inner and outer point and interaction point constraint. Then interpolation is performed between these two points. If the interpolation succeeds we have at least three layers in the game and we're dealing with what is named a *track segment* and has all the track parameters defined by a fitting procedure. If the interpolation fails, we move on to consider the next inner point (2).

4. For each segment a list of compatible vertex points is created and for each of them interpolation from the 'outer' point to the vertex region is attempted. For the successful associations extrapolation to the outer SCT layers is performed and both tracks are offered as a replacement for the best track candidates (primary and secondary) found for the current outer point.

5. When all the combinations for a given outer point are exhausted the time comes to assess the new candidates (if any). The TRT association is attempted for the primary candidate and if it succeeds the truncated and secondary candidate are bluntly deleted and the new born primary is checked for ambiguities against the existing list of tracks upon insertion into the list of found tracks. Otherwise the truncated candidate (subjected to the same ambiguity check) is inserted into the track list and the secondary track is inserted into the list of pending secondaries.

At the end of the road processing the list of pending secondaries is scrutinized. Special care is taken to make the best possible TRT association for each group of the ambiguous secondary candidates.

As combinatorial searches can become very inefficient if they are taken too literally, the inner workings of `iPatRec` take special care not too replicate the effort i.e. duplicated tracks produced by the combinatorial search are suppressed in the moment their duplicity becomes obvious. This is essential if `iPatRec` is to be useful in the computationally intensive trigger environment.

Information available to `ieElRec`

`ieElRec` is entered at the end of each road processing. Its main input parameters are the road's center and width in η and φ together with the track list originating from the preceding track reconstruction package. `ieElRec` is independent of the seeding method used as it searches through the data produced by the ECAL and HCAL reconstruction for clusters lying within the road. Therefore the first level reconstruction entities used in `ieElRec` are:

- the list of tracks produced by `iPatRec`;
- access to the list of ECAL clusters and
- access to the list of HCAL clusters.

It is worth mentioning that the HCAL clusters include the energy deposited in the ECAL.

Another input to `ieElRec` is of a completely different nature. As already argued in several passages of Sec:3.1, matching the track parameters projected to the ECAL with the corresponding EM cluster provides valuable information. Another aspect of the EM clusters turned out to be of great importance in the pion rejection: namely the depth profile of the EM shower and leakage into the hadronic calorimeter. To get a good parameterization of these quantities a large sample of single electrons and positrons was produced in the $1.5\,\mathrm{GeV} \leq \mathrm{p_T} \leq 60\,\mathrm{GeV}$ energy range. The distribution of the generated events was flat within the range $-2.5 \leq \eta \leq 2.5$. Additionally, a smaller sample of single pions was also produced to measure the pion rejection efficiency. The produced data-sets with respective sample sizes are tabulated in Tab:3.9. All these productions were carried out with the "Physics TDR layout" and with the realistic magnetic field. Please note that all the data samples used for the "Physics TDR" were generated using a constant field approximation.

Energy [GeV]	No. $e^{\pm}$ [k]	No. $\pi^{\pm}$ [k]
1.5	60	12
2	60	12
3	60	12
5	40	2
10	30	2
20	30	2
30	20	2
40	20	2
50	12	2
60	10	2

Table 3.9: $e^{\pm}$ and $\pi^{\pm}$ single particle productions. All event samples are equally split into the particle/antiparticle halves.

For each of the $e^{\pm}$ event samples the following six quantities were histogrammed for all primary tracks found by `iPatRec`:

1. $\delta\varphi \sim -\mathrm{sgn}(\mathrm{p_T})(\varphi^{\mathrm{E}} - \varphi^{\mathrm{iPat}})$ the difference in φ of the EM cluster and track's projection to the ECAL. The sign of track's p_T was used to correct for differences between the electrons and positrons;

2. $\delta\eta \sim \eta^{E} - \eta^{\mathrm{iPat}}$ the difference in η of the EM cluster and track's projection to the ECAL;

3. $\delta p \sim 2(E_T^E - |p_T^{\mathrm{iPat}}|)/(E_T^E + |p_T^{\mathrm{iPat}}|)$ the difference between transverse energy measured by the ECAL and absolute value of the momentum measured in the tracker normalized by the mean energy of the EM cluster and the track;

4. $\delta E_1^2 \sim E^2/E^1$ the ratio of energies measured in the second and first sampling of the ECAL;

5. $\delta E_s^3 \sim E^3/E$ the ratio of energies measured in the third sampling of the ECAL and all the energy contained within the EM cluster;

6. $\delta E_e^h \sim E^H/E^E$ the ratio of energies measured in the HCAL and ECAL cluster.

All samples were divided into seven $|\eta|$ bins with the fences posted at the values 0, 0.3, 0.6, 1.0, 1.4, 1.8, 2.2 and 2.55. A look-up table was constructed out of the mean values and rms's of the distributions (quantities 2 and 3 were fitted with a Gaussian and the mean value and standard deviation used instead). The δX symbols will be used for the normalised residuals in later discussion. Fig:3.13 gives an example of these distributions.

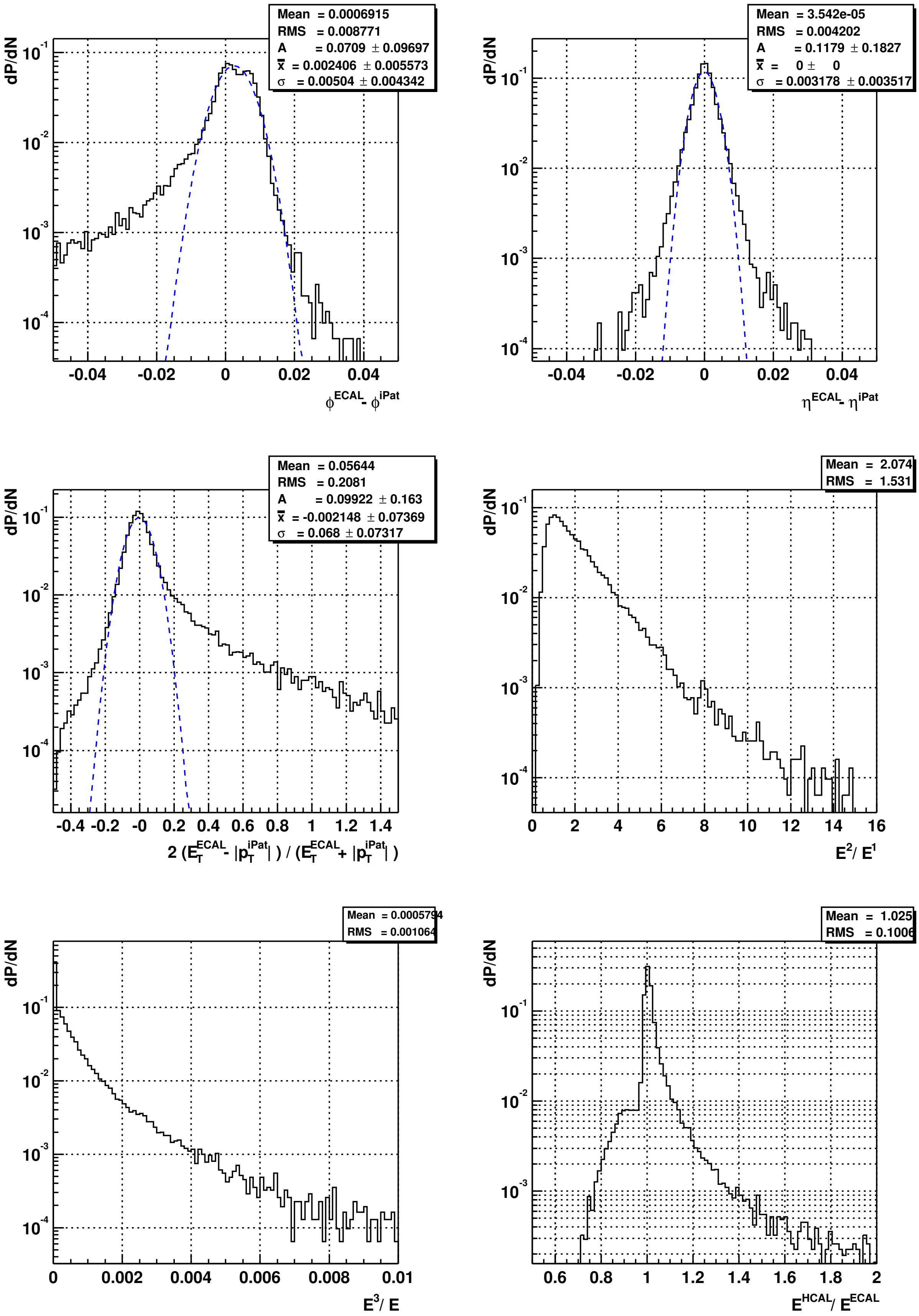

Figure 3.13: Examples of the distributions of quantities relevant for the electron reconstruction (see text for details). The sample used was $p_T = 5\,\mathrm{GeV}$ $e^{\pm}$s over all ID η. For the first three plots the Gaussian fit is superimposed.

3.2.2 Description of `ieElRec`

As already mentioned `ieElRec` itself is invoked for each of the roads analysed by `iPatRec`. But as the roads can be overlapping, the notion of an event is also known to `ieElRec`. In the same spirit as `iPatRec` produces list of tracks in road as its output, `ieElRec` outputs a list of electron candidates equipped with additional information. A detailed account of the information provided will be given by the end of the description.

Per event chores

Initialization of `ieElRec` is basically just re-initialization of the electron candidate container. It is then filled with the candidates coming from roads and a cross check is made if a candidate with the same ID track is already in it. If it is, the better one is kept. The meaning of *better* will become more obvious in later sections.

Road processing

First a list of ECAL clusters compatible with the current road is created and sorted by the cluster energy. This helps in resolving the ambiguities when several EM clusters are produced by a single electron with a hard bremsstrahlung. Then a loop over the clusters is entered. In it, three things happen.

1. The HCAL cluster that encompasses the ECAL cluster is searched. Especially at low energies there may be no HCAL association.
2. Pre-selection of tracks matching the cluster is made and the isolation is studied.
3. The detailed analysis is performed, followed by the selection and tagging of the tracks that made it through the needle's eye.

The details follow …

Preselection is done in two steps. As we are selecting tracks from a road that can be much wider than reasonable for EM clusters, the first check excludes all tracks not satisfying the $|\eta^E - \eta^t| < 0.1$ cut. Passing this cut the normalized residuals for the track–cluster pair are produced from the look-up table (see the enumeration in Sec:3.2.1) and stored in a hash map for faster processing. At the same time χ^2 per degree of freedom is calculated for the first three variables (the ones with explicit dependence on the track parameters).[1] The tracks that are to pass are subjected to the following cuts:

- $|\delta\eta| < 50$ This cut is harmless to the electrons and is in some regions even looser than pre-pre-selection cut on the η matching. We need it to be rather large as isolation determination is based on the number of preselected tracks.
- $\chi^2 < 2500$ This one looks entirely out of proportion. Yet there are still some electrons that fail it miserably. These are the cases with more than 50% energy loss by the end of the pixels. Although there is not much hope for such deviant cases they're kept for their contribution to the electron identification.

[1] Its probability distribution is far from the χ^2 thingy known from the books about statistics as the original distributions are not Gaussian. It is used in the same sense however … and also computed in the same way. Hence the name was kept.

Tracks of each kind (primary, truncated and secondary) are kept in separate containers. Each of the containers is sorted by $|\delta\eta|$ so that the more probable candidates will be processed first. Remember that matching in η is not spoiled by a bremsstrahlung.

Next the number of primary and truncated tracks is summed. If several tracks are found it means we're in a jet. This is important as different cuts are used for isolated and non-isolated tracks. Also … if we're dealing with an isolated track we can afford a little more magick and recuperate the hard bremsstrahlung cases which produced two or more EM clusters. The procedure relies on the fact that in this case the HCAL cluster contains all of them properly weighted. (As mentioned before, the ECAL reconstruction applies per cluster corrections and merging them directly would lead to an even bigger error.) But there is still a chance of a neutral hadron making an invisible contribution to the HCAL cluster. Here is the collection of cuts that help us evade this possibility:

- $1 < E^H/E^E < 2.5$ Remember that EM clusters are sorted by energy and that we're targeting at merging two or at most three clusters.
- $\mathsf{rms}(\eta_H) < 0.06$: the spread of HCAL's cluster energy in η should be small. Both of these cuts are also targeted at the suppression of further processing of hadrons that left some of their energy in the ECAL. Their typical signature is a large $E^{\mathrm{HCAL}}/E^{\mathrm{ECAL}}$ and a width in η around 0.1.
- The EM clusters with their centers within $\eta_H \pm 2 \times \mathsf{rms}(\eta_H)$ and $\varphi_H \pm 2 \times \mathsf{rms}(\varphi_H)$ are searched for and their energy added to that of the current cluster. The sum of the EM energy should fulfill the requirement $1.1 \times \sum_{i\in\mathrm{cut}} E_i^E > E^H$.
- In case when no additional EM clusters are found and we have an electron candidate, the above cut is replaced by a requirement that matching to the HCAL cluster is better than to the ECAL one. This recovers catastrophic bremsstrahlung cases in the last layers of the SCT or in the TRT.

If all these happens to be true the current EM cluster is replaced by the content of the HCAL cluster and the rest of the EM clusters that were used up are wiped out of the road's list. As this procedure has certainly disrupted the residuals for our electron candidate, they are recalculated.

Primary cuts are applied to the preselected tracks before they enter the inner mechanism of `ieElRec`. For isolated tracks they are:

$$|\delta\eta| < 10 \quad \wedge \quad \chi^2 < 100 \qquad \text{or} \qquad |\delta\eta| < 4. \tag{3.2}$$

Of course, for the second variant the pre-selection χ^2 cut still applies. In jets we're a bit more picky as it is hard to estimate the authenticity of the EM cluster:

$$|\delta\eta| < 6 \quad \wedge \quad \chi^2 < 100. \tag{3.3}$$

These cuts are only applied to the primary and truncated tracks. Having a truncated track that passed the cuts, a matching secondary is searched for and attached onto its tail.

Candidate scrutinization is the core of `ieElRec`. Its logic is based on the results presented in Sec:3.1 and a later fine–tuning on the problematic events.

Pixel, Head and SCT fits of the track are built first. The pixel fit contains the first three measurements and the head fits are obtained by a successive addition of the layers up to the last SCT measurement. If the candidate is a truncated track, the head fits outside of candidate's original hits are suppressed (if a secondary is attached, its hits form a prolongation through the SCT into the TRT). The SCT fit is done for all hits belonging to the SCT. In case of a truncated track without an associated secondary it can happen that there isn't enough measurements available.

It was attempted to use the pixel $r\varphi$ residuals of the SCT fit for the early bremsstrahlung detection but mean values of the obtained distributions were negligible compared to their spread. Therefore no information could be extracted from them.

Selection of the best track fit is a bit trickier than anticipated due to the effects of multiple scattering. Three cases are considered in the following order:

1. **Pixel-only fit** is accepted if:

$$\chi^2_{\mathrm{pix}} < \chi^2_{\mathrm{i}} \quad \wedge \quad |p_T^{\mathrm{pix}}| > |p_T^{\mathrm{i}}|, \qquad \text{for all i,}$$

   where index i applies to the head fits.

2. `iPatRec` **fit** (primary or truncated) is taken if multiple scattering effects are obvious. The SCT fit must exist for further consideration and its p_T measurement must yield a larger value than all the head fits:

$$|p_T^{\mathrm{sct}}|/|p_T^{\mathrm{i}}| > 1.015 \quad \wedge \quad \chi^2_{\mathrm{sct}} > \chi^2_{\mathtt{iPatRec}}, \qquad \text{for all i.}$$

   Index i iterates over head fits.

3. **Head fit** with the smallest χ^2 is selected otherwise.

Candidate labeling provides the tracks with information about the detected bremsstrahlung, quality of matching with the ECAL cluster and pion ambiguity level. In most of the cases the goodness of match and bremsstrahlung type are closely correlated. The information available is scarce and heavily hidden under the rug of multiple scattering so it is hard to provide but the most general information. Regarding the bremsstrahlung `ieElRec` separates four cases: no relevant bremsstrahlung (`B1`), a hard bremsstrahlung photon emission in the pixels(`B2`) or in the SCT(`B3`). The last case is a possible catastrophe(`B-1`), a very hard bremsstrahlung occurring in the beam-pipe or b-layer which results in a failure of extrapolation of the track into the b-layer.

ECAL/ID matching is based on the cuts in the δp-$\delta\varphi$ plane. Again one cannot do much magick without producing spurious artefacts. The following enumeration presents the possible cases and their respective cuts. The first matching case is accepted.

M1 **Good match** corresponds to the cuts $|\delta p| < 3 \ \wedge\ |\delta\varphi| < 3$. There exists a subset of these events that does not associate to the b-layer and members of which are candidates for an early catastrophic bremsstrahlung. To differentiate between the two cases, we label the events with the b association as **M1b** and bremsstrahlung type `B1`, while those without the b association get a bremsstrahlung type `B-1`.

It is possible to get a sample with a 'cleaner' p_T signature by further narrowing of the residual cuts. As these are the *representative* sets of events, the b-layer association is required. Later we will study two subsets in further detail:

M1b$^+$ with cuts $\delta p < 1 \ \wedge \ \delta\varphi > -1$ and

M1b^{++} with cuts $\delta p < 0 \ \wedge \ \delta\varphi > 0$.

M2 Imprecise ECAL. Especially at low energies, where the tracker is still precise, it is quite frequent to get a good p_T measurement but not too good match with the EM cluster. These cases are obtained by applying the cut $-3 < \delta p < 1 \wedge -10 < \delta\varphi < -3$. Bremsstrahlung type remains undetermined.

M3 Poor ID corresponds to an early bremsstrahlung in pixels where only a poor p_T measurement can be made. The applied cuts are: $\delta p > 1 \ \wedge \ \delta\varphi < 3$. Quite obviously, this corresponds to the `B2` brem-type.

M4 Poor ECAL is a variation on the theme of **M2**, enhanced by a post p_T measurement hard bremsstrahlung which causes the electron to spiral way to far in φ. The cut is $\delta p < -3$. No cut is applied to φ as it can become basically anything. Many pions sneak through this classification but are later identified by the longitudinal profile of the EM cluster. Bremsstrahlung wise, these are labeled as `B3`

M0 Unknown ... which simply means that the event has failed all the above options.

Pion ambiguity (A_π) is expressed as a signed integer obtained by summing together the *pion/anti-pion signals*. They are extracted from the track's behaviour, the TR information and EM cluster properties.

1. A weight of $|\delta p|/3$ is assigned to candidates originating from a primary track with $\delta p < -3 \ \wedge \ \delta\varphi > -3$. This signals a "missing" energy in the ECAL without a brem correlation which would suggest $\delta\varphi < 0$.

2. Selection of the pixel fit is considered an anti-π signal with a weight -1.

3. The TR information contributes a weight in the range from 2 to -2 and is based on percentage of the TR hits. Inner fences are posted at 5%, 10%, 16% and 26%; e.g., tracks with 10 to 16% of the TR hits are assinged a weight of 0.

4. Each of the longitudinal EM residuals (δE_1^2 and δE_s^3) contributes a weight of +1 if $\delta E > 3$ and a weight of +2 if $\delta E > 6$.

This served mostly as an introduction as the relevance of these categories can only be proven in action. Also ... it introduced the nomenclature and notation.

3.3 Results for single electrons

`A notational convenience:` throughout this section p_T and E_T are shamelessly used as shorthands for "p_T (or E_T) measurement provided by `ieElRec`". Please note that these symbols are also used as "the true transverse energy". In dubious cases they are set as E_T^{true} or p_T^{true}.

For all results presented in this section, the reduced ECAL clustering cut of $E_T^{\mathrm{EM}} = 0.7\,\mathrm{GeV}$ was used for $E_T^{\mathrm{true}} \leq 5\,\mathrm{GeV}$ (see Sec:3.1.5).

3.3.1 Efficiency

As already mentioned the electron reconstruction inefficiency at low energies is dominated by the EM reconstruction (see Tab:3.3). In all following discussion the efficiencies are quoted for the events that produce an EM cluster. In more than 99% of cases an inefficiency of `ieElRec` is in fact an inefficiency of `iPatRec`. And again ... most of these can be attributed to a disastrous bremsstrahlung.

The first thing of interest is *Electron identification efficiency.* It should be interpreted as: if we have an isolated ECAL cluster produced by an electron, what is the probability of finding and assigning an ID track to it. The dependence of efficiency on transverse energy and $|\eta|$ is shown in Fig:3.14. The efficiency is increasing with E_T as there is less and less probability for a catastrophic bremsstrahlung to cause the electron to spiral along the magnetic field before obtaining the minimum number of position measurements. The $|\eta|$ dependence follows the material distribution. In the very last bin we can observe a drop in the efficiency as we are approaching the limit of the ID coverage.

Another thing is how well these electrons are reconstructed. For an analysis that needs electron tracks reconstructed with a high precision the electron reconstruction efficiency is only the first step toward obtaining a good electron sample. Fractional decomposition into the types of track matching can now be enumerated. For its true meaning one should combine these fractions with resolutions that accompany them, and that will be discussed in later sections.

The table showing the efficiencies/probabilities (Tbl:3.10) grew quite large. It is not my intention to overwhelm the reader but rather to provide the detailed information for cross-checks and comparison with other reconstruction programs.

3.3.2 p_T resolution and E/p

Overview of match types

For warm-up, let us begin with some raw p_T^{true}/p_T distributions. The intention is to make an overview of the different ID/ECAL matching types and to further classify the events that failed to make a good association (aka **M1**).

Comparison of all the reconstructed tracks to those that make a good match (**M1** and **M1b**$^{++}$ classes) is shown in Fig:3.15. The important thing is that the bremsstrahlung tails are effectively suppressed by the application of the cuts. Purity of the **M1** samples is better at higher energies where the effects of the multiple scattering are negligible. Further analysis of the mean values, resolutions and tail content will be made later when studying the E_T/p_T distribution.

E_T	η	ECAL	`ieElRec`	M1	M1b	M1b$^+$	M1b^{++}	M2	M3	M4	M0
1.5	all	70.91	93.31	81.91	76.87	66.75	28.12	2.69	1.43	4.05	3.24
	barrel	84.89	96.67	82.17	78.89	66.57	27.81	2.19	0.34	5.80	6.17
	transition	52.62	93.07	79.70	74.01	64.02	28.67	4.69	0.42	4.85	3.40
	endcap	97.02	90.62	84.30	78.50	70.15	27.73	0.74	3.60	1.54	0.44
2	all	89.12	94.23	79.20	74.04	64.03	27.46	3.36	2.70	6.15	2.81
	barrel	97.72	97.01	79.54	76.07	64.70	26.11	3.11	0.86	8.86	4.64
	transition	80.35	93.60	77.49	71.95	61.41	25.93	5.15	0.72	7.33	2.92
	endcap	99.66	92.60	81.88	75.72	67.96	31.46	0.47	7.98	1.43	0.84
3	all	97.08	95.30	78.93	74.35	64.56	29.00	3.24	4.75	6.20	2.17
	barrel	99.98	97.65	80.34	77.95	66.81	26.07	2.26	1.37	10.25	3.44
	transition	94.45	94.55	77.35	72.19	62.33	27.31	5.25	2.64	6.81	2.50
	endcap	99.87	94.46	80.78	75.17	66.89	35.45	0.09	12.53	0.86	0.20
5	all	99.30	96.28	82.16	78.71	69.90	35.45	2.27	6.98	4.03	0.84
	barrel	100.00	98.30	85.49	83.72	74.35	32.65	2.35	3.09	6.21	1.17
	transition	98.65	95.90	82.13	77.88	68.90	34.38	3.30	4.86	4.56	1.05
	endcap	99.97	95.05	78.86	75.39	67.50	40.55	0.02	15.40	0.71	0.07
10	all	99.86	97.08	85.20	83.02	74.13	41.67	0.68	9.27	1.77	0.17
	barrel	99.99	98.56	88.62	87.21	78.65	39.53	1.23	5.53	2.96	0.21
	transition	99.82	97.02	86.53	83.78	74.88	42.41	0.74	7.67	1.85	0.22
	endcap	99.83	95.75	78.95	77.28	68.06	42.19	0.01	16.37	0.41	0.00
20	all	99.99	97.88	86.20	84.87	75.79	44.43	0.04	10.47	1.14	0.03
	barrel	99.99	99.34	90.65	89.49	80.37	42.93	0.08	6.78	1.80	0.03
	transition	100.00	97.74	87.29	85.67	77.12	46.82	0.04	9.32	1.05	0.04
	endcap	99.96	96.68	79.25	78.39	68.16	40.70	0.00	16.79	0.65	0.00
30	all	100.00	98.34	86.35	85.31	75.72	44.99	0.00	10.85	1.12	0.02
	barrel	100.00	99.05	89.68	88.57	78.76	43.24	0.00	7.50	1.83	0.04
	transition	100.00	98.58	88.00	86.79	77.74	48.16	0.00	9.65	0.92	0.01
	endcap	99.98	97.08	79.31	78.72	68.14	39.81	0.00	16.95	0.83	0.00
40	all	99.98	98.54	86.50	85.58	75.93	44.91	0.00	10.80	1.25	0.00
	barrel	100.00	99.42	88.64	87.40	77.82	44.38	0.00	8.69	2.09	0.00
	transition	100.00	98.69	87.71	86.74	77.57	47.54	0.00	9.90	1.07	0.00
	endcap	99.94	97.33	81.64	81.17	70.37	39.62	0.00	14.93	0.76	0.00
50	all	99.98	98.77	86.56	85.66	76.56	44.68	0.00	10.99	1.23	0.00
	barrel	100.00	99.39	87.93	86.50	76.23	41.55	0.00	9.32	2.14	0.00
	transition	100.00	99.01	87.71	86.83	78.43	49.08	0.00	10.23	1.07	0.00
	endcap	99.93	97.57	82.53	82.14	72.73	38.12	0.00	14.42	0.61	0.00
60	all	100.00	98.89	86.83	86.02	76.43	45.85	0.01	10.86	1.19	0.00
	barrel	100.00	99.68	89.45	88.54	77.31	44.84	0.05	8.29	1.90	0.00
	transition	100.00	99.01	87.86	86.94	77.64	47.75	0.00	10.13	1.01	0.00
	endcap	100.00	97.85	81.95	81.49	72.88	42.74	0.00	15.03	0.87	0.00

Table 3.10: Efficiencies relevant for `ieElRec` (all given in %). For completeness the ECAL reconstruction efficiency and electron indentification efficiencies are also presented. Types of matching (**Mx**) are explained in Sec:3.2.2. Please note that cases under **M1x** are subsets of **M1**. η regions used are the same as throughout Sec:3.1: barrel $\sim\ |\eta| \leq 0.6$, transition $\sim\ 0.6 < |\eta| \leq 1.9$ and end-cap $\sim\ |\eta| > 1.9$.

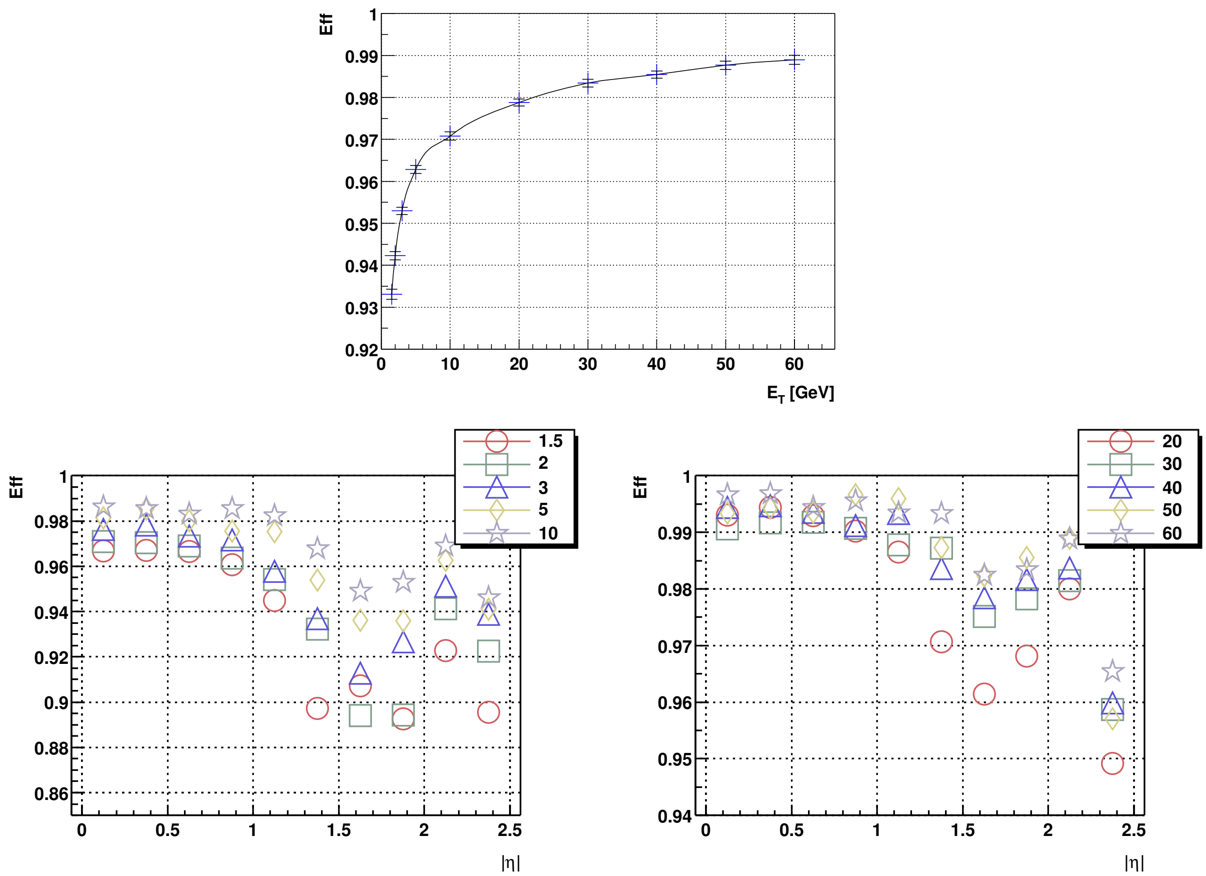

Figure 3.14: Electron identification efficiency of `ieElRec` versus transverse energy over all ID coverage (top). Efficiencies versus $|\eta|$ for different transverse energies (left: E_T from 1.5 to 10 GeV, right: 20 to 60 GeV).

Next we consider match types **M2** and **M4** which are supposedly only relevant at lower energies. Raw $p_T^{\rm true}/p_T$ distributions for low energies are presented in Fig:3.16. To give a more quantitative description one should combine the fractional probabilities (Tab:3.10) with Fig:3.17, which shows mean values and rms's of both $p_T^{\rm true}/p_T$ and $E_T/E_T^{\rm true}$.

M2 is occurring only up to $E_T \sim 20$ GeV with a fractional probability of about 2%. We see that both p_T and E_T are underestimated on average and that the p_T measurement *is* better over all region of validity. At $E_T = 20$ GeV this match type becomes very unlikely so the statistics for these entries in Fig:3.17 is insufficient ($\sim$ 12 events).

M4 is suppressed by the ECAL clustering cut at very low energies (up to 2 GeV) where one would expect it to flourish. So it peaks at 5% for $E_T \sim 3$ GeV and then falls to slightly above 1% for transverse energies above 10 GeV. Note that the p_T measurement is satisfactory up to 20 GeV and that the E_T measurement is quite bad. Also note that the E_T measurement is of approximately the same quality as p_T at 30 GeV which implies that the **M4** match type should only be considered seriously up to this energy.

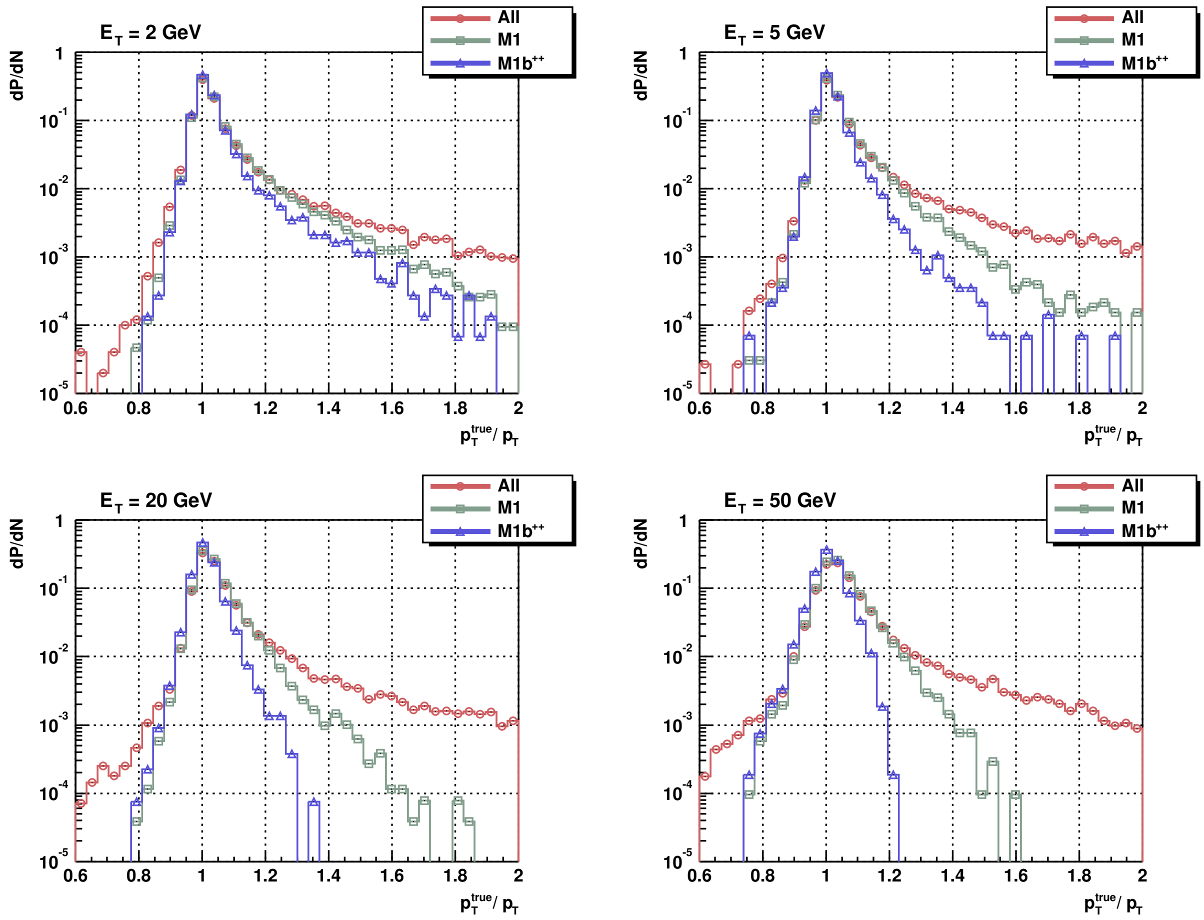

Figure 3.15: p_T^{true}/p_T distributions of all electron tracks and match types **M1** and **M1b**$^{++}$ for transverse energies 2, 5, 20 and 50 GeV.

M0 has a certain relevance up to $E_T \sim 10\,\mathrm{GeV}$ with a fractional probability at the 1% level. Both the p_T and E_T are underestimated. The p_T is better up to $E_T \sim 2.5\,\mathrm{GeV}$ where the E_T measurement takes over with an under-estimation of the energy of about 15%.

M3 corresponds to a poor p_T measurement. Its fractional probability starts low ($\sim 1\%$) at $E_T = 1.5\,\mathrm{GeV}$ and increases steadily to $\sim 10\%$ at 20 GeV where it takes over the event classes belonging to **M2** or **M0** at lower energies. For higher energies it remains constant at the same level. Consider Fig:3.18 which presents the details of the p_T and E_T measurements. p_T is indeed poor over all energy range. By considering also all the events and **M1** (Fig:3.15) one can observe that a large fraction of the bremsstrahlung tails is slurped into the **M3** category. As we're dealing with the early bremsstrahlung cases it is no surprise that the E_T measurement is also spoiled at lower transverse energies where bending power of the solenoidal field is sufficient to split the electron–photon pair. This effect becomes negligible at $E_T \sim 30\,\mathrm{GeV}$.

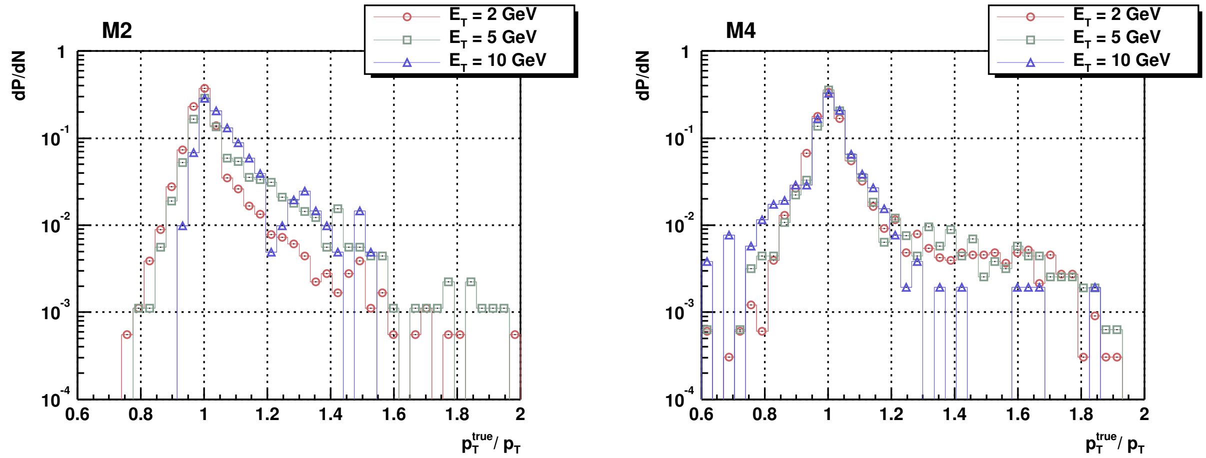

Figure 3.16: $p_T^{\rm true}/p_T$ distributions of match types **M2** and **M4** for transverse energies 2, 5 and 10 GeV.

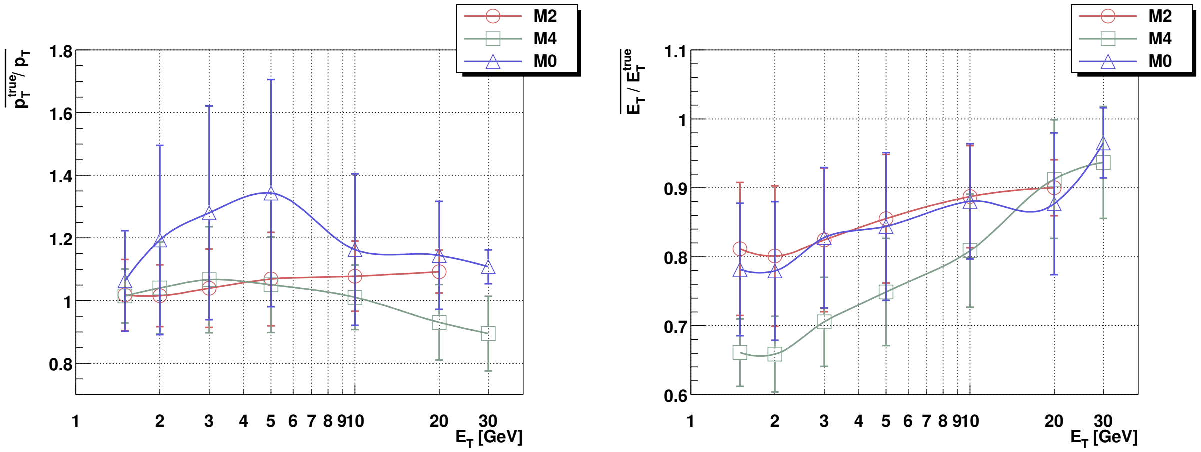

Figure 3.17: The mean values and rms's (error bars) of the $p_T^{\rm true}/p_T$ (left) and $E_T/E_T^{\rm true}$ (right) distributions versus transverse energy. The match types shown are **M2**, **M4** and **M0**.

Improvement of the p_T measurement by `ieElRec`

As `iPatRec` is desperately trying to make the tracks as long as possible it is not infrequent for it to overshoot beyond reasonable limits. The method of accepting one of the head-fits (see Sec:3.2.2) is trying to correct this feature as it is a bug in case of electrons. To estimate if it is doing any good, the following quantity was studied:

$$\Delta_{p_T}^{\tt ieElRec} = \frac{|p_T^{\rm true} - p_T^{\tt iPatRec}| - |p_T^{\rm true} - p_T^{\tt ieElRec}|}{|p_T^{\rm true}|}. \tag{3.4}$$

This quantity measures the difference of the p_T mismatch for the track candidate obtained from `iPatRec` and for the final electron fit chosen by `ieElRec`. Positive values mean improvement of the p_T measurement and the negative ones a degradation. Fig:3.19 shows the behaviour of $\Delta_{p_T}^{\tt ieElRec}$. There is a strong η dependence (following the material distribution) and the average improvement of the p_T is increasing from about 1% at $E_T = 1.5$ GeV to 4% at 60 GeV. The **M3** case gives a better correction but it shouldn't be taken too seriously

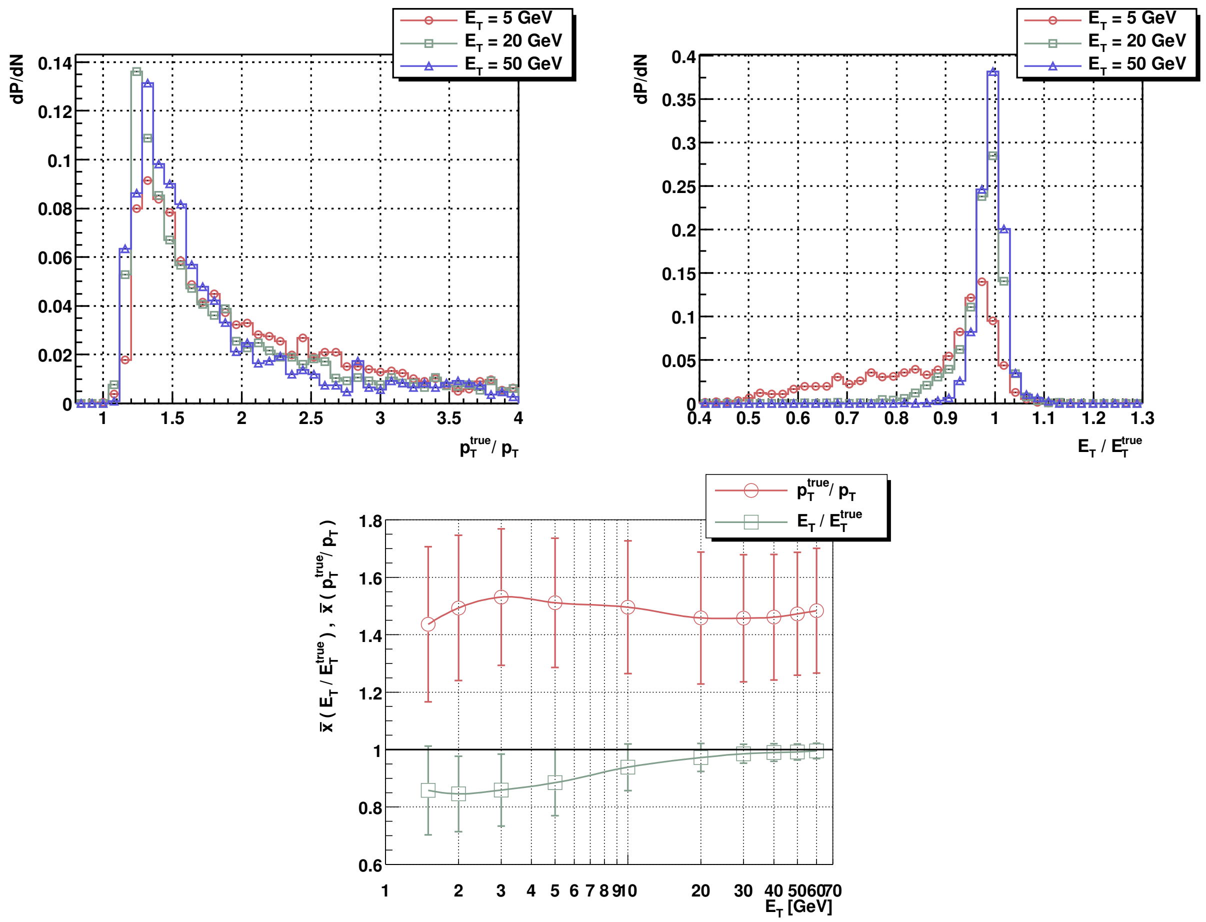

Figure 3.18: Scrutinization of **M3**. Top two plots show raw p_T^{true}/p_T and E_T/E_T^{true} distributions for typical energies. Note that x-axis scales are radically different. The bottom one presents mean values and rms's of the two distributions versus E_T.

as the p_T measurement is screwed in this case anyway and can't be resurrected but with a divine intervention.

Resolutions, E/p and tailers

Let us give some further consideration to the p_T^{true}/p_T and E_T/E_T^{true} distributions for good match types. To arrive to the statistical description, the distributions were fitted with a Gaussian curve in a $\pm 2 \times$ rms range around the center. The mean values and resolutions obtained in this way are shown in Fig:3.20. As far as the p_T measurement is concerned, improved matching types (**M1b**$^+$ and **M1b**$^{++}$) provide a progressively better mean value and resolution. For the E_T measurement the mean value of **M1b**$^{++}$ is slightly less good at low energies (up to $E_T \sim 10\,\mathrm{GeV}$). The p_T resolutions for **M1b**$^+$ and **M1b**$^{++}$ are better in this energy range and **M1b**$^+$ provides a good compromise between the E_T and p_T accuracy.

For those searching the best energy measurement available, we can summarize the results in the following points. For $E_T \leq 10\,\mathrm{GeV}$ the p_T measurement is better, regardless of the type of matching. In the intermediate energy range ($10\,\mathrm{GeV} < \mathrm{E_T} \leq 30\,\mathrm{GeV}$) the p_T measurement is better for events belonging into **M1b**$^{++}$. Otherwise the E_T measurement is better. At higher energies ($E_T > 30\,\mathrm{GeV}$) the E_T measurement is always better.

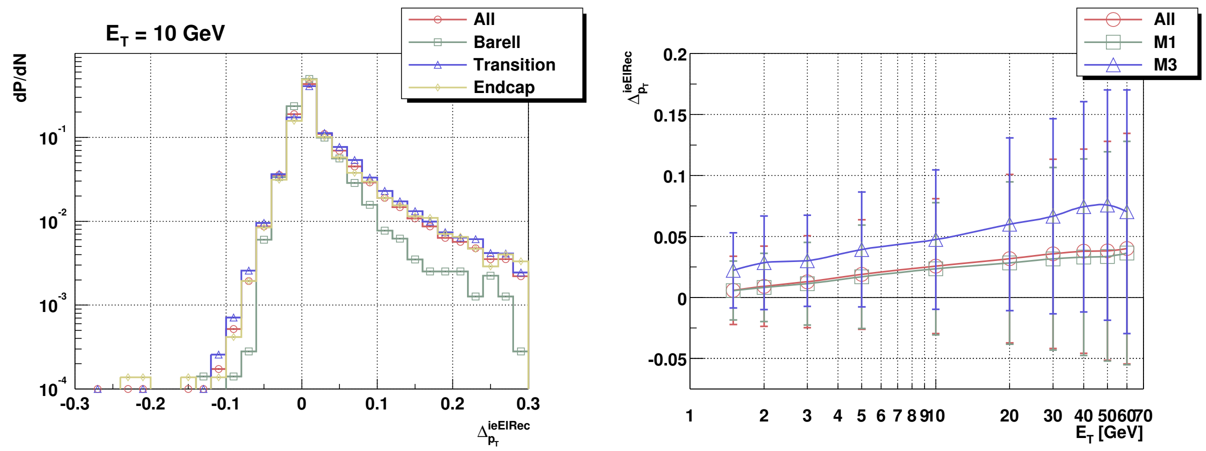

Figure 3.19: Behaviour of the $\Delta_{p_T}^{\mathtt{ieElRec}}$ parameter. Raw distributions for all events and for the three $|\eta|$ regions are shown for $E_T = 10\,\mathrm{GeV}$ (left). Dependence of the mean value and rms on the transverse energy is given in the right plot.

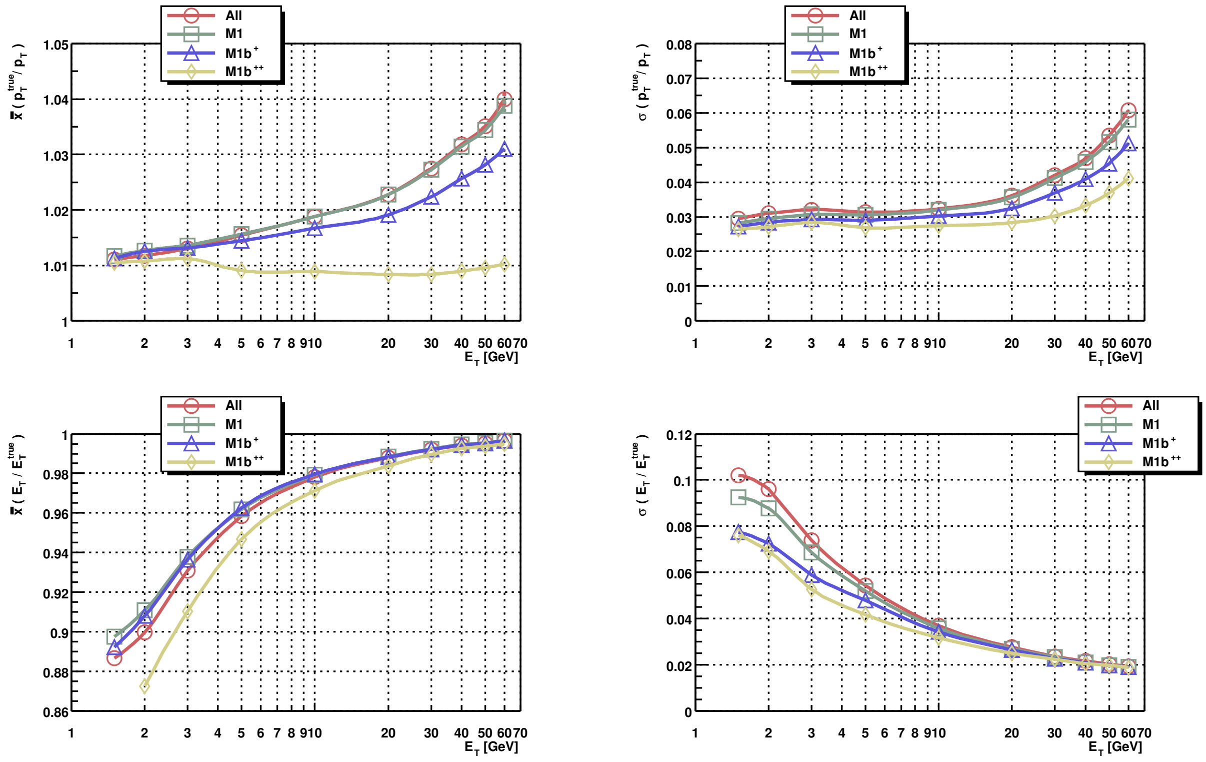

Figure 3.20: The mean values (left) and resolutions (right) of the p_T^{true}/p_T (top) and E_T/E_T^{true} (bottom) versus the transverse energy.

The $|\eta|$ dependence of the parameters of Gaussian fits to the p_T^{true}/p_T and E_T/E_T^{true} distributions is shown in Fig:3.21. Plots for $E_T = 5, 40\,\mathrm{GeV}$ are chosen as the representatives for the two energy regions. Basically what we're looking at is the material distribution which is in the case of $\bar{x}(E_T)$ modulated by all the bremsstrahlung misfortunes mentioned before.

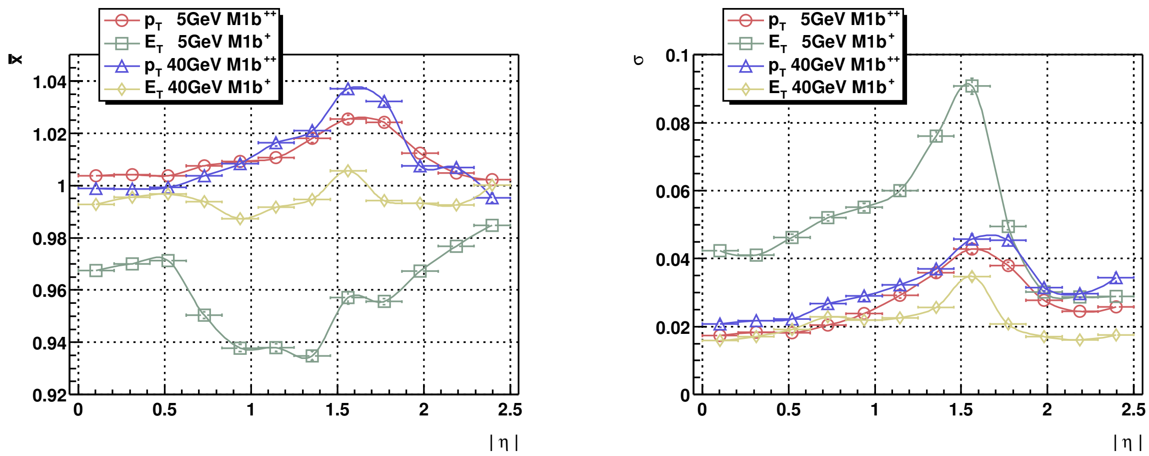

Figure 3.21: $|\eta|$ dependence of the mean values (left) and resolutions (right) of the$p_T^{\rm true}/p_T$ and $E_T/E_T^{\rm true}$ distributions for $E_T = 5, 40\,\mathrm{GeV}$. $\mathbf{M1b}^{++}$ and $\mathbf{M1b}^{+}$ samples were used for obtaining values for the p_T and E_T respectively (as labeled).

The E_T/p_T distribution is considered the fruit of all the foregoing work. First it is valuable in identifying the electrons. This fact has been used in `ieElRec` by use of the δp variable. Second, it serves as an important source for the calibration of the ECAL. Events from the $Z^0 \to ee$ decays will be used for this purpose. While it can be a source of a stand-alone ECAL calibration, it also enables the calibration by the ID. As bremsstrahlung is standing in our way, we need a good detector description and bremsstrahlung simulation. The precise peak positions, as well as the resolutions, and their dependence on E_T and η must be known. (See [2], Sec:7.2.2.) With this weapon in our hands, we can also use the $W^\pm \to e\nu$ events.

To obtain these values the cores of the E_T/p_T distributions were fitted with a Gaussian. Fig:3.22 shows the E_T dependence of the parameters. At low transverse energies (up to $10\,\mathrm{GeV}$) the mean value behaviour is dominated by a too low E_T measurement caused by the 3×7 cluster window size. At higher energies the mean value is following the shift of the p_T distribution due to bremsstrahlung. The resolution of the E/p is of course a merging of the two underlying distributions (as in $\sigma_{E/p}^2 = \sigma_E^2 + \sigma_p^2$) and is again dominated by the ECAL at low energies and tracker at higher energies. The seemingly unnatural improvement of the resolution at $E_T = 1.5\,\mathrm{GeV}$ is due to the suppression of the hard bremsstrahlung events by the ECAL clustering cut.

The $|\eta|$ dependence is shown in Fig:3.23. As it was the case for the E_T and p_T distributions, the material effects are the most important. At lower energies the offset from unity is ECAL dominated (therefore decreasing the mean value of the E/p), while the tracker takes the responsibility at higher energies (increasing the mean value).

Fractions of events in the tails is another big concern. It is `ieElRec`'s responsibility to filter them out and to prove that it is doing a good job we plotted the contour lines of the E_T/p_T distributions (cumulated along each $|\eta|$ bin) in Fig:3.24.

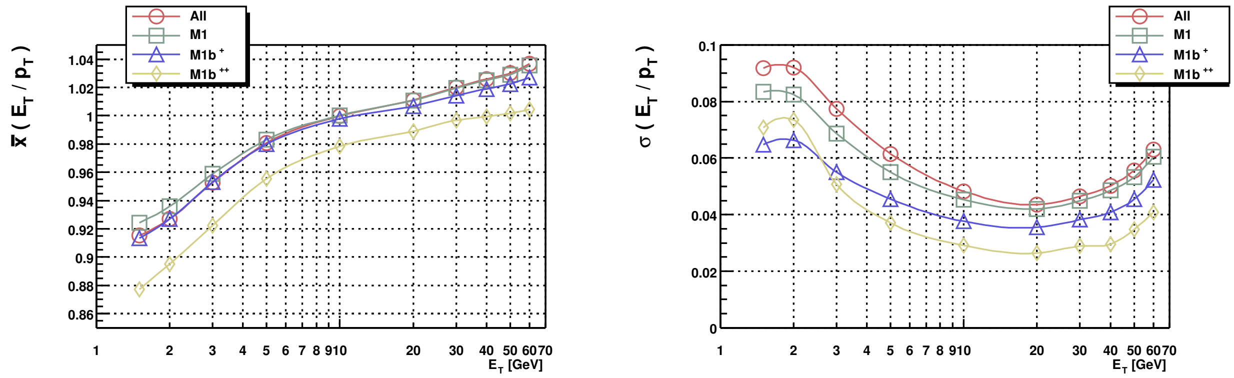

Figure 3.22: Mean values (left) and resolutions (right) of the E_T/p_T distribution versus transverse energy.

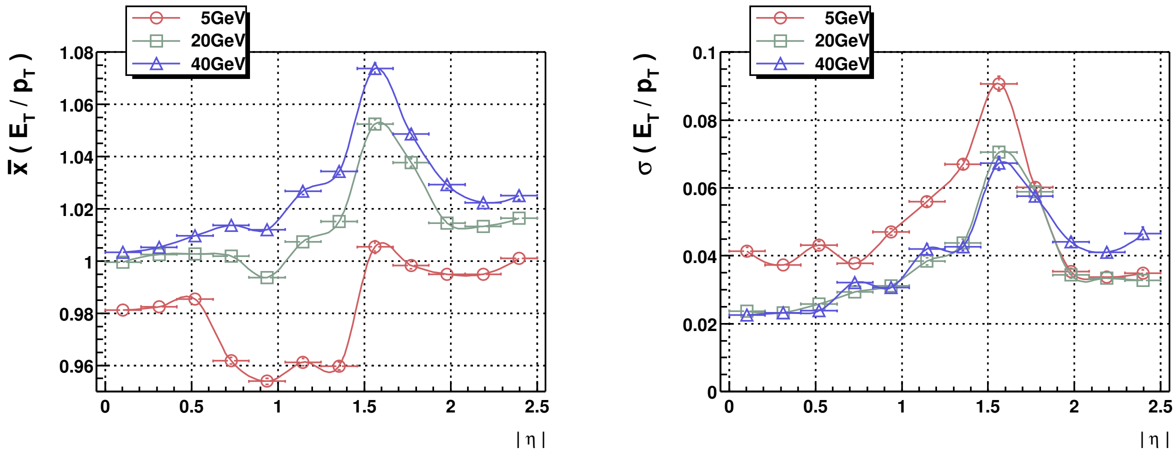

Figure 3.23: $|\eta|$ dependence of the mean values (left) and resolutions (right) of the E_T/p_T distribution. Transverse energies 5, 20 and 40 GeVare shown for the match type **M1b**$^+$.

3.3.3 Impact parameter resolution

Determination of the impact parameter is important for secondary vertex reconstruction (e.g., B decays), heavy flavour tagging, lifetime measurements and association of the track to the correct primary vertex at high luminosity. The measurement of impact parameter is dominated by the first few layers i.e. the pixel detector. Since the pixel pad size is 6 times larger in z than in r-φ direction, the resolution in the transverse direction is much better. At lower energies multiple scattering contributes most uncertainty to the measurement. It can be approximated by a const/$\mathrm{p_T}$ power law. For a further discussion and comparison see [5], Sec:4.4.

Transverse impact parameter (a_0) resolutions as functions of the transverse energy and $|\eta|$ are shown in Fig:3.25. The variation of the resolution with the match type is minimal and is improving with increasing transverse energy. As the first few layers are dominating the resolution and unnatural prolongation of tracks in the transverse direction leads to a degradation of measurement, one expects an improvement of the resolution by the usage of the truncated tracks. To quantify and prove this assertion resolutions for original tracks are

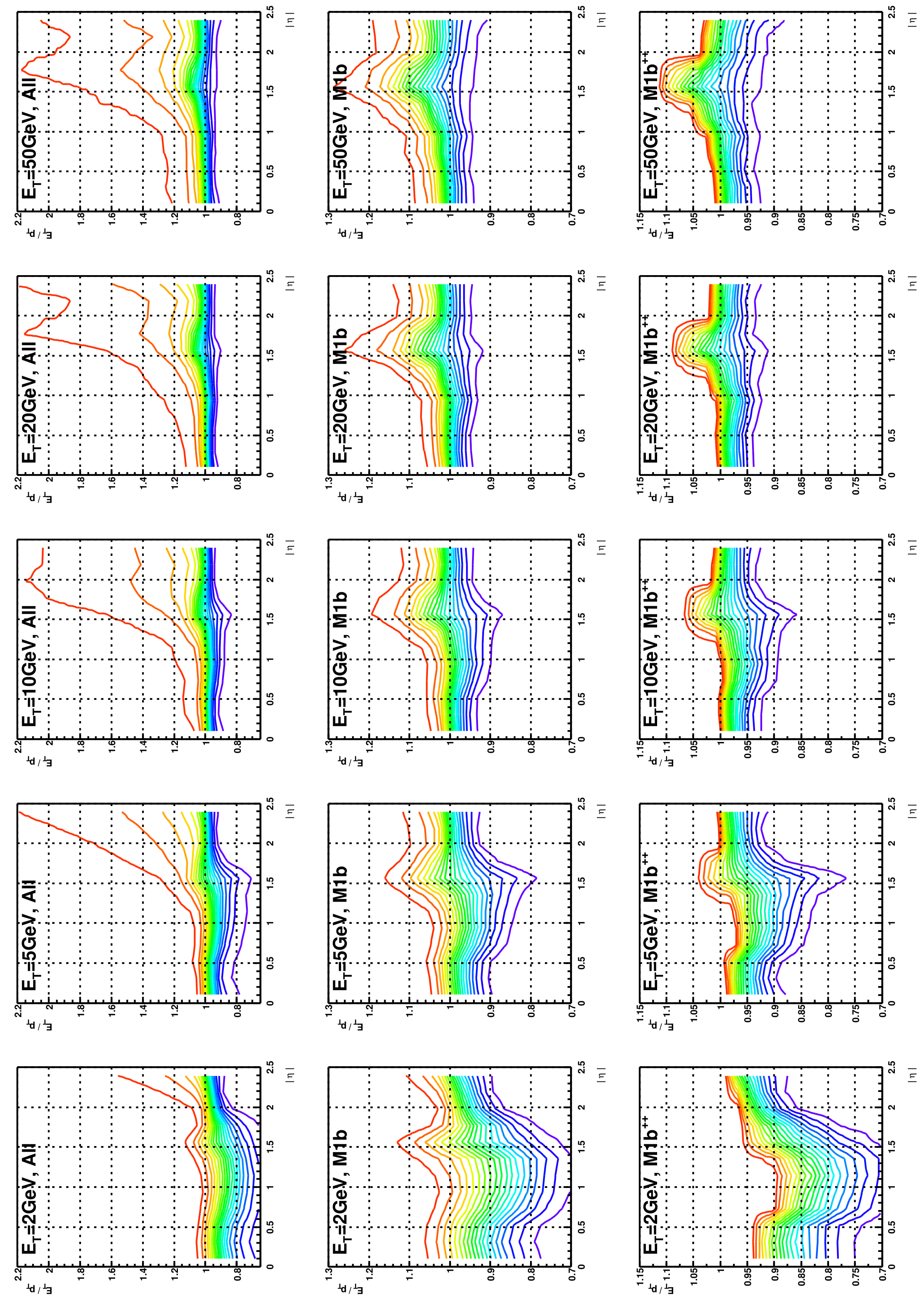

Figure 3.24: 5% contour lines of the E_T/p_T distributions for different transverse energies (row-wise). Curves are shown for all the events and for the match types **M1b** and **M1b**$^{++}$ (column-wise). y axis scales are different for each event selection!

also plotted versus $|\eta|$. The effect is of course most pronounced in the regions with highest amount of material where it improves the resolution by about 15%.

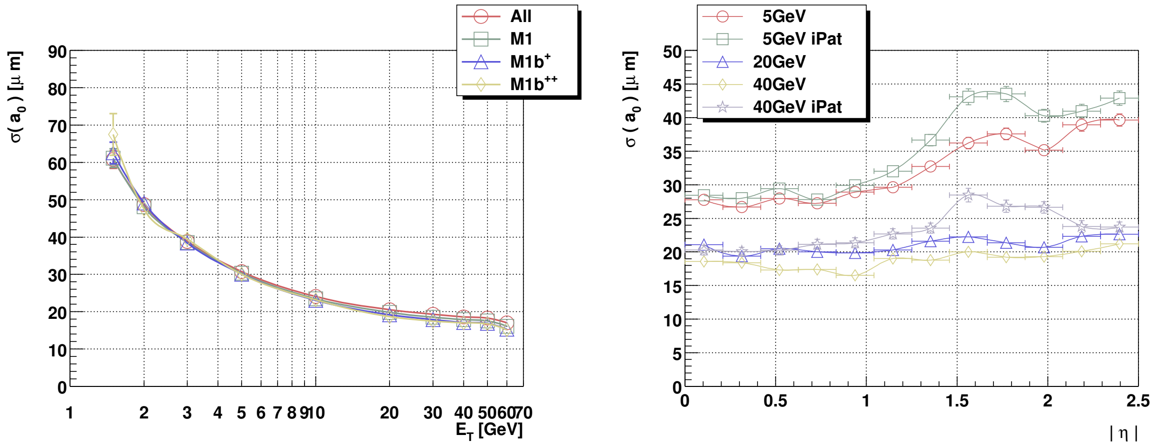

Figure 3.25: Resolution of the transverse impact parameter a_0. E_T (left) and $|\eta|$ (right, match type **M1b**$^+$) dependencies are shown. The curves labeled by iPat correspond to the resolutions obtained from seed tracks coming from `iPatRec` (before possible truncation).

Logitudinal impact parameter (z_0) should, on the other hand, in principle benefit from longer tracks as track's direction in r-z plane is not influenced by the bremsstrahlung. By observing the same kind of plot as for a_0 (Fig:3.26) we must discard this hypothesis as the resolutions are basically unaffected. Again there is no dependence on the match type.

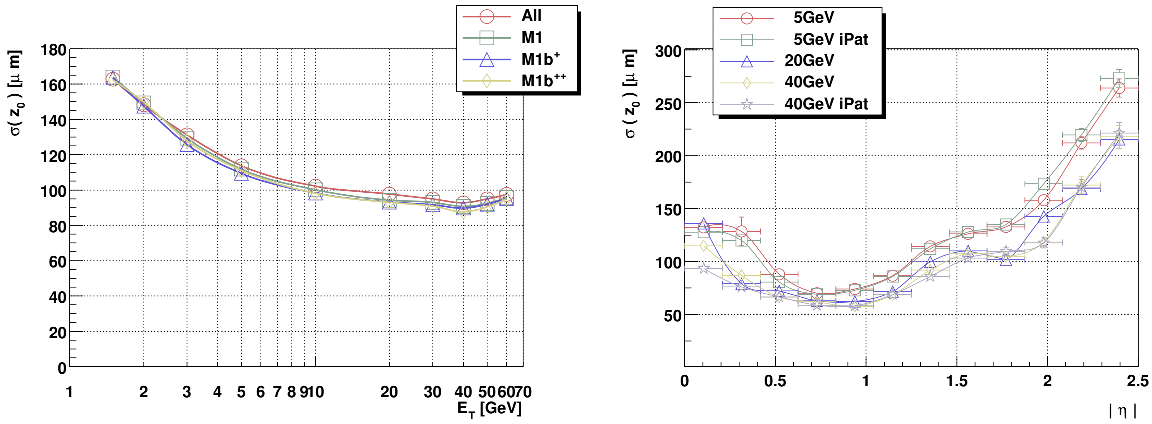

Figure 3.26: Resolution of the longitudinal impact parameter z_0. E_T (left) and $|\eta|$ (right, match type **M1b**$^+$) dependencies are shown. The curves labeled by iPat correspond to resolutions obtained from seed tracks coming from `iPatRec` (before possible truncation).

3.3.4 Angular resolution

The direction of the track at the vertex point plays a crucial role in the measurement of an invariant mass. It is expressed by two angles: φ is measured in the transverse plane (x-y) and θ in the r-z plane. It is more practical to consider the $\cot\theta$ as this equals p_z/p_T. The transverse energy dependence can again be parameterized by $A + B/p_T$. As the φ measurement is sensitive to bremsstrahlung, its η dependence follows the material distribution and is improved by the usage of the truncated tracks (Fig:3.27).

For the $\cot\theta$ measurement the resolution is constant in the barrel and then degrades with η when we shift into the end-cap region where r is measured with a fixed resolution. No significant worsening of the resolution by the track truncation can be observed (Fig:3.28).

For comparison with the muon tracks see [5]:Sec:4.3.

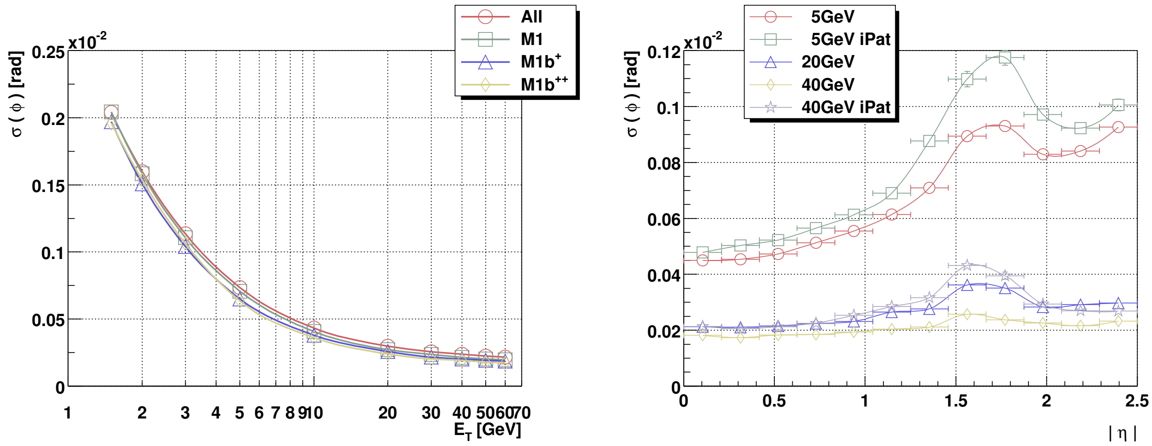

Figure 3.27: Resolution of ϕ. E_T (left) and $|\eta|$ (right, match type $\mathbf{M1b^+}$) dependencies are shown. The curves labeled by iPat correspond to the resolutions obtained from the seed tracks coming from `iPatRec` (before possible truncation).

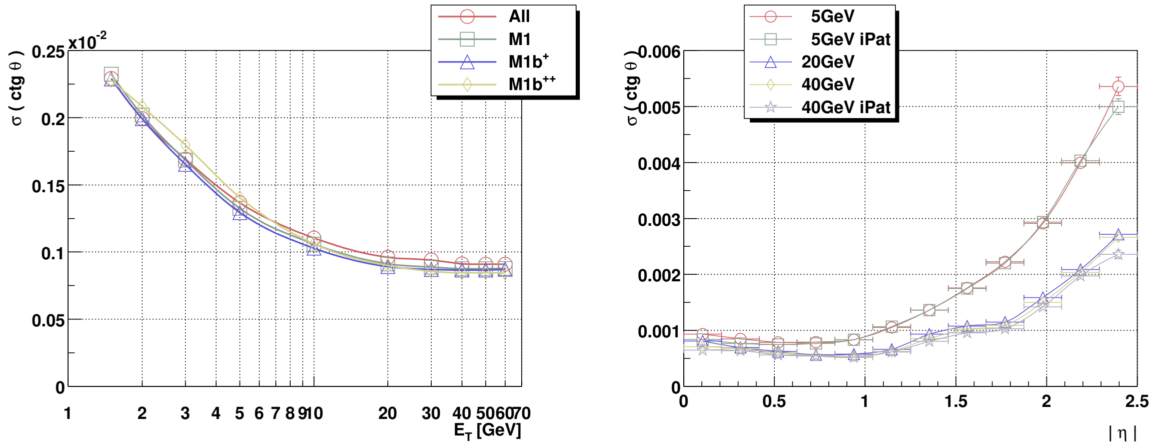

Figure 3.28: Resolution of $\cot\theta$. E_T (left) and $|\eta|$ (right, match type $\mathbf{M1b^+}$) dependencies are shown. The curves labeled by iPat correspond to the resolutions obtained from the seed tracks coming from `iPatRec` (before possible truncation).

3.4 Pion rejection

For all the results presented in this section, the reduced ECAL clustering cut of $E_T^{\mathrm{EM}} = 0.7\,\mathrm{GeV}$ was used for $E_T^{\mathrm{true}} \leq 5\,\mathrm{GeV}$ (see Sec:3.1.5).

Charged pions can produce a large energy deposit in the ECAL via the formation of the Δ resonance which has a plentiful spectrum of excited states ($\pi^+ n \to \Delta \to \pi^0 p$ and $\pi^- p \to \Delta \to \pi^0 n$) in 1.2 to 3 GeVrange. The π^0 promptly decays into two photons and the misfortune occurs. The cross-section for this process is decreasing with energy and above 10 GeV sporadic low energy EM interactions prevail. These cases are then easy to spot by a large E_T-p_T mismatch. A more complete study of the electron/pion separation with emphasis on the trigger level application can be found in [2]:Sec:7.3.1. The basic difference is that while trigger's goal is assuring as high pion rejection as possible, `ieElRec` is trying to obtain very good electron efficiency at about 1% pion acceptance.

The variables used for obtaining the pion ambiguity A_π are discussed in Sec:3.2.2. But before we plunge into the rejections and efficiencies, some thought must again be given to the ECAL reconstruction efficiency. We saw that the ECAL is not fully efficient for electrons at low energies. And luckily it is not fully efficient for pions, either. Fig:3.29 shows fractions of pions and electrons that make it all the way through the `ieElRec` without applying any pion rejection cuts yet. As pion efficiencies are already lower, some part of the rejection has already been done. By futher requiring the electron candidate to be of the **M1** class, the π rejection factor is above 30 for 10 GeV and higher transverse enrgies. In what follows we will consider the electron efficiency to be 100% if all the electrons passing the `ieElRec` processing also pass the rejection cuts. In the same spirit we will not count the pions that fail `ieElRec` (mostly by not producing the EM cluster) to be successfully rejected. Therefore we will be studying the internal `ieElRec` rejection. To come to the absolute values one should combine this information with the values extracted from Fig:3.29.

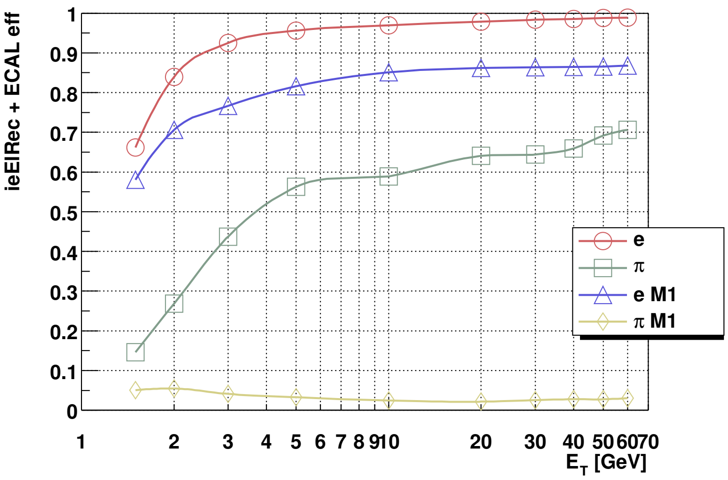

Figure 3.29: Efficiencies for electrons and pions to pass the `ieElRec`'s processing and making it into the electron candidate class.

The most interesting things happen in the range $A_\pi : -2 \nearrow 2$. The electron reconstruction and pion rejection efficiencies for these cases are shown in Tab:3.11. Note that a rather small number of the generated pion events (Tab:3.9) casts some shadows on the statistical value of the rejection factors. This is especially true for the pion rejection versus the electron inefficiency plot presented in Fig:3.30. The last point (with the highest rejection) for each curve was obtained by substituting the last entry with 100% pion rejection with the number of events that passed the pre-`ieElRec` cuts (therefore assuming that the next generated pion would be identified as an electron).

E_T [GeV]	e_{eff} -2	π_{rej}	e_{eff} -1	π_{rej}	e_{eff} 0	π_{rej}	e_{eff} 1	π_{rej}	e_{eff} 2	π_{rej}
1.5	0.405	1.000	0.803	0.998	0.938	0.987	0.986	0.970	0.997	0.899
2	0.428	1.000	0.826	0.998	0.946	0.987	0.987	0.975	0.997	0.925
3	0.456	1.000	0.839	0.998	0.951	0.983	0.988	0.975	0.997	0.946
5	0.471	1.000	0.850	1.000	0.957	0.996	0.990	0.988	0.997	0.959
10	0.491	1.000	0.854	1.000	0.961	0.984	0.992	0.980	0.998	0.959
20	0.487	1.000	0.843	1.000	0.958	0.984	0.991	0.975	0.998	0.955
30	0.495	1.000	0.846	1.000	0.958	0.990	0.991	0.981	0.998	0.954
40	0.481	1.000	0.831	1.000	0.952	0.987	0.989	0.979	0.997	0.956
50	0.474	1.000	0.827	1.000	0.951	0.985	0.989	0.974	0.997	0.947
60	0.471	1.000	0.826	0.999	0.954	0.987	0.990	0.975	0.998	0.938

Table 3.11: Electron reconstruction and pion rejection efficiency for the relevant values of A_π.

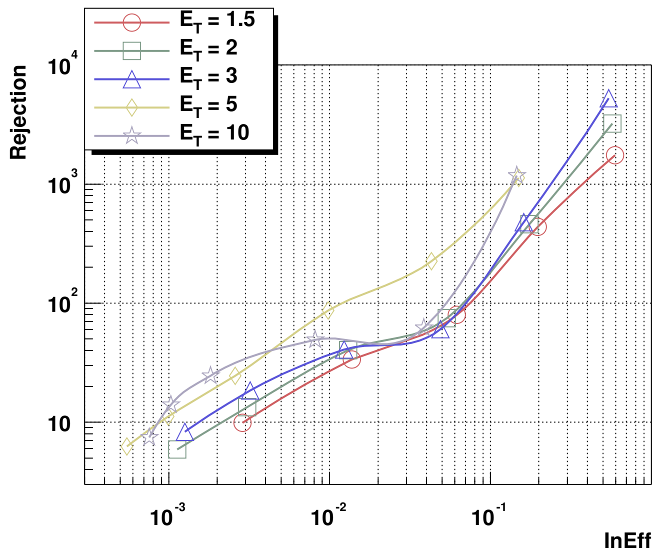

Figure 3.30: Pion rejection versus electron reconstruction inefficiency for different values of E_T.

3.5 Reconstruction in jets

So far we have been only considering isolated electrons. In this section we review the relevant quantities for electrons in jets. To cover a wide range of track multiplicities, we used the $B^0 \to J/\Psi \to ee$ event sample. The same event sample was used for the analysis presented in 4.1, where it is discussed in more detail. The important details are that the p_T of e's was forced to be above 2 GeV and the $|\eta|$ cutoff was 2.5. The distributions are shown in Fig:3.31. Total number of $e^{\pm}$'s was 62700. For this study the ECAL clustering cut (explained in 3.1.5) was set to $E_T = 1\,\mathrm{GeV}$ for all transverse energies.

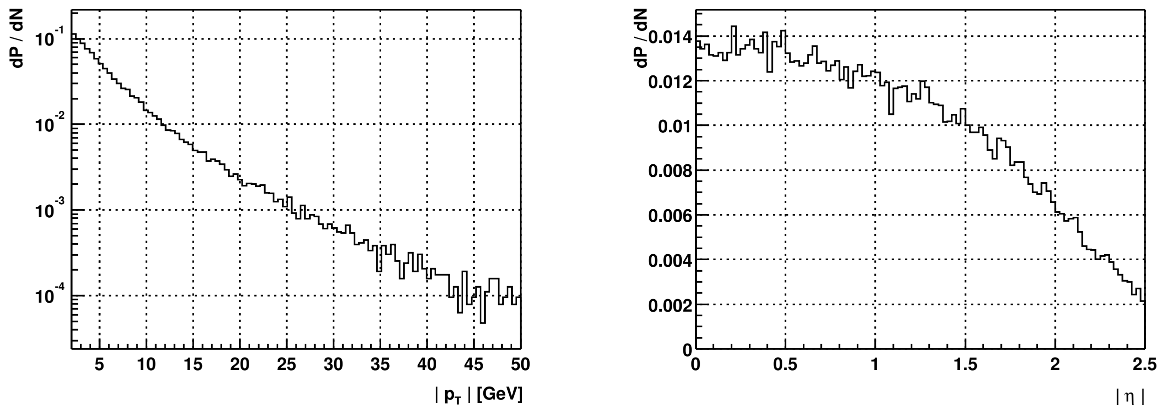

Figure 3.31: Distributions of generated $|p_T|$ and $|\eta|$.

Some deteriorations in `ieElRec`'s performance are expected to occur. They can be attributed to a degradation of `iPatRec`'s reconstruction efficiency and higher occupancy of the ECAL, which results in poorer resolutions of all its measurements. Also, more stringent selection cuts are applied inside `ieElRec` when it suspects to be running inside a jet (Sec:3.2.2). It is also true that most of the lost electrons are of poor match type, i.e., we cut them out as the ECAL information is possibly polluted. As we're interested in how well we can find and tag good electrons, we study the `ieElRec`'s efficiency and ECAL's purity for different track multiplicities. Plan of attack would be slightly different if we were interested in the electron/jet separation. This topic is covered in the 'Physics TDR' ([2]:Sec:7.4).

To determine the track multiplicity (N_T) information from the event generation record was used. Given an electron track, we first searched for the matching HCAL cluster. Then all the charged particles with $p_T > 1\,\mathrm{GeV}$ that projected into that cluster within $\eta^{\mathrm{HCAL}} \pm 2 \times \mathsf{rms}_\eta^{\mathrm{HCAL}} \;\wedge\; \varphi^{\mathrm{HCAL}} \pm 2 \times \mathsf{rms}_\varphi^{\mathrm{HCAL}}$ were counted. Fig:3.32 shows the distribution of multiplicities 'measured' this way. To retain statistical plausibility, we individually considered multiplicities up to $N_T = 7$. The rest were analysed in one bunch (marked as 8^{++}). The second plot on the same figure shows the mean value and rms of the distribution obtained by histogramming the sum of p_T of neighbouring tracks divided by the true p_T of the electron versus the multiplicity of the event.

To further differentiate the event sample we separately studied the three $|\eta|$ regions: barrel (32.1% of events), transition (56.6%) and end-cap (11.3%). As the ECAL's efficiency is varying significantly within the p_T range covered by the generated electrons, we also studied three p_T regions: $|p_T| < 4\,\mathrm{GeV}$ (39.0%), $4\,\mathrm{GeV} \le |\mathrm{p_T}| < 10\,\mathrm{GeV}$ (43.6%) and $|p_T| \ge 10\,\mathrm{GeV}$ (17.4%).

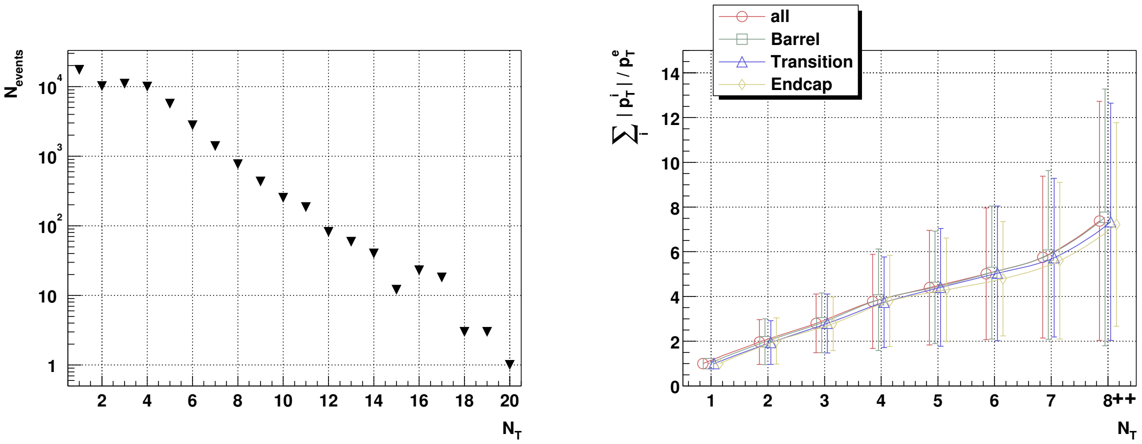

Figure 3.32: Left: number of available events for a given value of track multiplicity. Right: Average p_T^{jet} of a jet normalized to the electron p_T. The error bars show the rms's of the distributions.

3.5.1 `ieElRec`'s efficiency

As ECAL's efficiency is studied separately, here we only consider events for which the EM cluster was successfully reconstructed. `ieElRec`'s efficiency as a function of the track multiplicity is shown in Fig:3.33. Compared to resultus for single particles, about 4% drop in efficiency can be observed over the available N_T range, without much deviations for different $|\eta|$ and p_T regions.

The `iPatRec`reconstruction efficiency (added to the right plot of Fig:3.33) in jets could be affected by a higher occupancy of the silicon detectors and possible shared hits. But, as can be seen, there is no observable effect. Tracks reconstructed by `iPatRec` were required to be either primary or truncated with majority of hits belonging to the *true* track in question. No cuts on ECAL association were applied.

The decrease of efficiency due to the *jet cuts* inside `ieElRec` can be determined by comparing the presented results to the efficiencies obtained for single particles (Sec:3.3.1). No change can be observed.

Another thing of interest is how the different match types partake in the multi-pie. Fractional contributions for all match types are shown in Fig:3.34. The most noticeable variation is the raise of the **M3** match type (i.e., poor p_T measurement by the tracker) for about 10% over the studied region. To a smaller extent ($\sim 2\%$) **M0** is also raising. On the other hand, to compensate for this raise, fractions of **M1** ($\sim 8\%$), **M2** ($\sim 1.5\%$) and **M4** ($\sim 2.5\%$) decline accordingly.

As there is no reason for the electrons to behave differently in jets and there is no observable change in `iPatRec`'s efficiency, we are led to the conclusion that the efficiency loss of `ieElRec` is caused by the more stringent cuts and ECAL pollution. On the other hand, migration of events into more dubious categories is entirely due to the degradation of ECAL performance.

3.5.2 ECAL pollution

First we study the efficiency of the EM cluster reconstruction. It is a bit problematic to define it for the non-isolated tracks as the cluster searching algorithm is looking for local

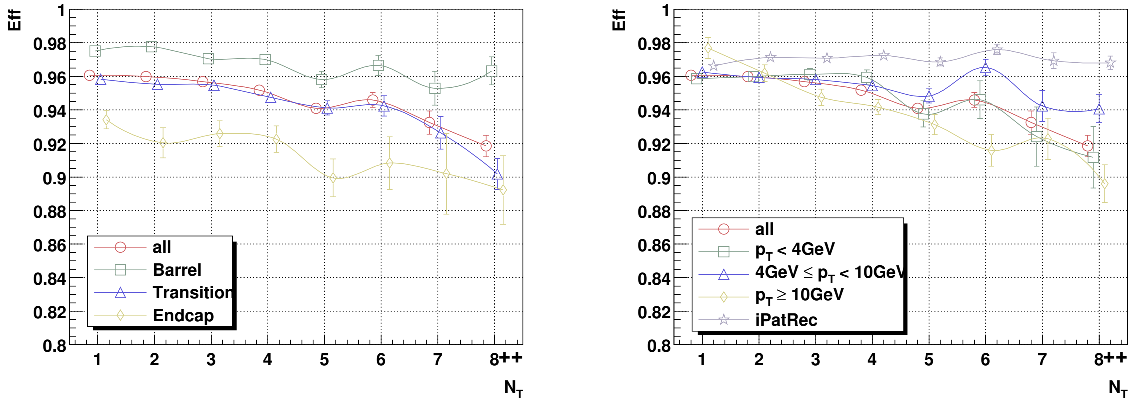

Figure 3.33: `ieElRec`'s efficiency as a function of the track multiplicity. $|\eta|$ regions are shown on the left plot. The right plot shows efficiencies for the p_T regions and also efficiency for `iPatRec` to find a primary or truncated track (no additional quality cuts applied).

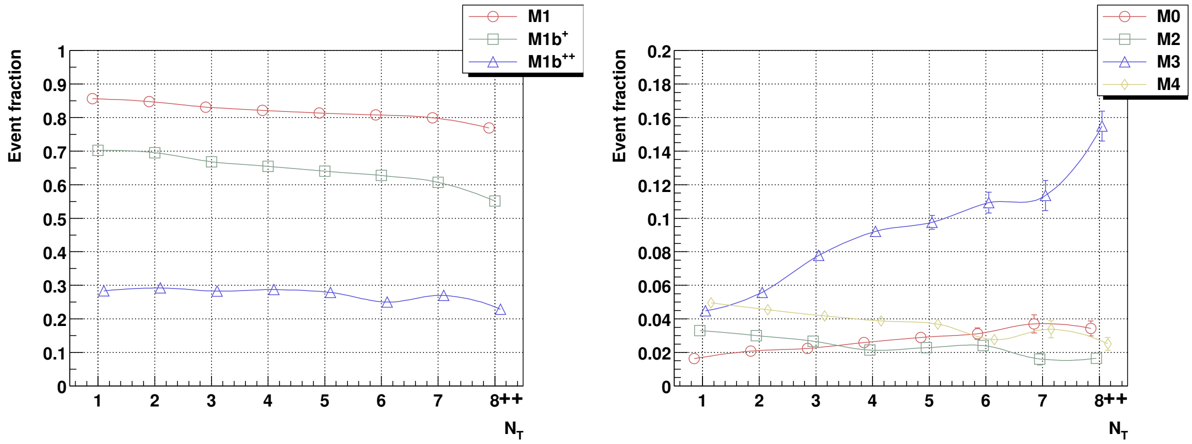

Figure 3.34: Fractions of events belonging to the different match-types as a function of track multiplicity. Good match types are shown on the left and the others on the right plot. y-axis scales are different.

maxima on the cell grid and can therefore fail to separate two closely lying tracks. Since we're only interested in cases where electron assignment can be made unambiguously (with reasonable tolerances), we consider the ECAL to be efficient in the following two cases.

1. `ieElRec` succeeds in finding the electron (EM clusters are used as seeds for `ieElRec`).

2. An EM cluster is found around the spot in ECAL to which the generated track projects to. The cut applied was (see Fig:3.13 for residual distributions):

$$4 \times \Delta\eta + \Delta\varphi \leq 0.15.$$

The results are presented in Fig:3.35. For transverse energies above 4GeV, where the ECAL is almost fully efficient, higher multiplicities only degrade the reconstruction efficiency. At lower energies additional depositions made by neighboring tracks first help the EM cluster to climb over the clustering threshold and only at multiplicities above $N_T > 4$ the efficiency begins its decline. Basically the same situation can be seen for the transition region ($0.6 < |\eta| < 1.9$), where the huge amount of material causes the ECAL to be more inefficient.

Another measure of the alien track conspiracy can be obtained by inspecting the behaviour of the mean value and spread of the E_T/E_T^{true} distribution as a function of the track multiplicity (Fig:3.36). While no specific η or p_T dependence can be observed, we can still estimate the average contribution of the neighboring tracks to the E_T measurement.

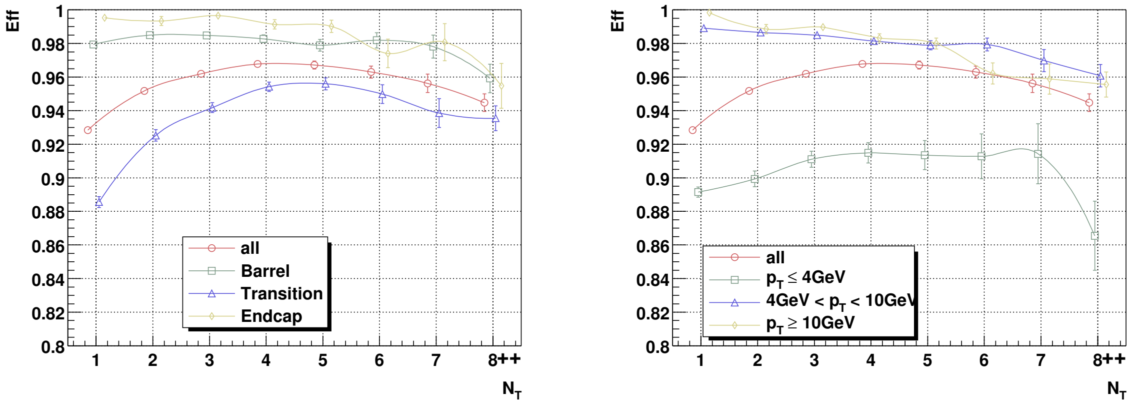

Figure 3.35: ECAL's efficiency as a function of track multiplicity. $|\eta|$ regions left, p_T right.

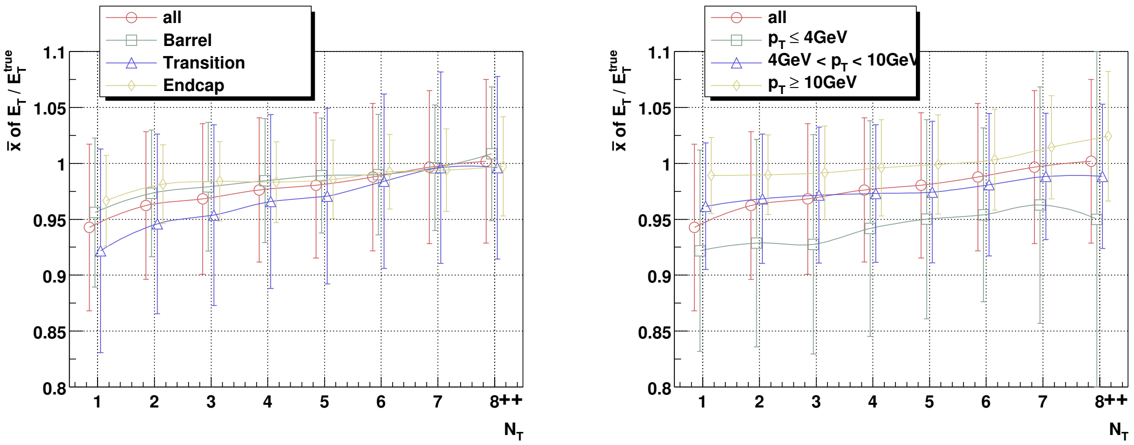

Figure 3.36: The mean values and resolutions (represented by error bars) of the EM clusters as a function of track multiplicity. $|\eta|$ regions left, p_T right.

3.6 Effects of pile-up

In contrast to the clean environment of lepton-antilepton colliders (such as LEP) the rich structure of colliding protons gives birth to many soft collisions for which the cross-section is many orders of magnitude larger than for the processes of interest ($\sim$ 100 mb to be compared to, say, H production with a cross-section of ~ 5 pb for $m_H = 500$ GeV). One of the design decisions for the LHC was to choose higher luminosity instead of higher energy and a multitude of minimum-bias events (as soft hadronic interactions are called) is the price that the LHC experiments must pay in terms of their operational environment. During the high-luminosity operation there will occur, on average (Poisson distributed), 23 such interactions in each bunch crossing. Luckily, many of the interaction products (and deflected protons) are emitted at low angles to the beam axis. As a rule of thumb, the number of particles is constant in each η interval up to $\eta \sim 6$. The average number is 7.5 charged particles (0.64 for a $p_T > 1$ GeV cut) and 9 neutral particles (90% of them are photons with the mean $E_T = 235$ MeV) per unit of pseudo-rapidity for one minimum-bias event. Another saviour comes in the flesh of the magnetic field which effectively curls up particles with $p_T < 0.5$ GeV so that they never make it to the outer parts of the detector. However, the tracker material produces a significant number of secondary interactions and conversions in front of the calorimeter.

Besides being a generic nuisance as a source of radiation damage and higher detector occupancy, minimum-bias events have a special pinch for sub-detectors with signal collection times longer than the time between consecutive collisions. Signals from several bunch crossings begin to overlap, both in space and time; this is called *pile-up*. From this perspective, the TRT and ECAL are the most heavily exposed parts of the ATLAS detector. Silicon vertex detectors have a ~ 20 ns shaping time and each of the electronic channels covers a very small area of the detector. In contrast, straws of the TRT are much longer and wider and, which is more important at the moment, the electron charge collection time in gas is about 60 ns, not to mention the ten times longer ion contribution, which has to be canceled out by the front end electronics. Even so, the expected TRT occupancy during the high-luminosity operation ranges from 15% to above 40%.

Things are even worse for the ECAL, where charge collection times can be as long as 500 ns (20 bunch crossings). Therefore, to correctly account for the effects of pile-up in the calorimeter, one has to superimpose about 500 minimum-bias events. Again, electronics is used to bypass the long collection time and to give a uniform 40 ns peaking time of the signal. While shaping can solve the problem of bunch crossing identification, a large contribution to the overall noise of the calorimeter is here to stay. For electrons, the most important piece of information is that pile-up contribution to the noise in the 3×7 window is ~ 300 MeV. Pile-up effects in the calorimeter are studied in detail in *Calorimeter Performance TDR* [8]:Sec:1.4.

There are other traps for electrons in the presence of pile-up than just the increase in noise. To stay with the ECAL associated problems, there will be random contributions to the reconstructed energy in the EM cluster belonging to an electron. This will inevitably lead to migration of some otherwise well reconstructed electrons to the **M3** match type or, even worse, to **M0** or even to fail the ID/ECAL association completely. Furthermore, some pattern recognition problems may be expected from the higher number of combinatorials. But things are far less tragic in this respect than generally believed. To quantify this statement note that while there are about the same number of tracks that pass the pre-selection cuts within `ieElRec` for the jet and pile-up data samples, the track multiplicity count, where a $p_T > 1\,\text{GeV}$ cut is applied, yields about 50% of events with a track multiplicity greater than one for the jet sample and only about 1% of events for the high-luminosity pile-up.

To study the effects of pile-up in detail, 2 000 events from the generated $e^{\pm}$ samples (1 000 e^{-}'s and 1 000 e^{+}'s) were merged with a high-luminosity pile-up using the standard procedures described in [2]:Sec:2.3. Electron samples with p_T up to 20 GeV were considered as no degradation in performance is expected above this energy.

More or less the same steps were taken as for the analysis of reconstruction in jets. Instead of studying the reconstruction efficiency and ECAL degradation as a function of track multiplicity, the dependency of both effects on the generated single electron p_T were be considered.

3.6.1 Efficiencies

As all along this chapter, EM clusters were used to define roads and initiate the ID reconstruction. The ECAL clustering cut was set to $E_T^{\text{EM}} \geq 1\,\text{GeV}$ for all event samples under study.

The first thing to note is that the ECAL reconstruction efficiency (as defined in Sec:3.5.2) increases at low p_T. The increase is 32% at $p_T = 1.5\,\text{GeV}$, 10% at 2 GeV and a bit more than 1% at 3 GeV. At 5 GeV the efficiency reaches the value obtained without pile-up. This can be partially understood by additional contribution of pile-up to an otherwise inefficient EM cluster which helps it crawl over the mark set by the clustering cut and therefore increases the ECAL reconstruction efficiency. The left plot of Fig:3.37 shows its dependence on p_T together with the electron identification efficiency of `ieElRec` and the reconstruction efficiency of `iPatRec`. Since EM clusters are used to seed the reconstruction, more is learned by studying efficiencies relative to the ECAL. Their E_T dependence is presented in the right plot of the same figure. The `iPatRec` curve starts above one at $p_T = 1.5\,\text{GeV}$, which means that the track gets reconstructed by virtue of a closely lying EM cluster produced by a track from a minimum-bias event or noise (a road half-width of $\Delta\varphi \times \eta = 45^{\circ} \times 0.1$ around the seed coordinate was used in ID reconstruction). This awakes further suspicion on the quality of reconstructed electrons at very low p_T, as can be seen from the efficiencies plotted for sub-selections of good (**M1**) and reasonably good (**M1**, **M2** or **M4** which all yield a good p_T measurement) electrons. Looking at the absolute scale, pile-up introduces a 5% drop in reconstruction efficiency for the **M1** match type at $p_T \leq 5\,\text{GeV}$, about a 2% drop at $p_T = 10\,\text{GeV}$ and above that the results are consistent with the data without pile-up.

To further investigate the effects of pile-up, the relative fractions of all match types were plotted versus E_T (Fig:3.38). The **M1** match type has already been discussed, it was observed that its relative fraction is below the one obtained without pile-up. The largest increase in fractional frequency is seen for the **M0** and **M3** match types. The first case corresponds to an ECAL cluster that can't be attached to an ID track in a reasonable way and therefore signifies EM clusters that have nothing to do with the electron. In contrast to those, the **M3** match type signals a lousy p_T measurement and in this case the transition is induced by an additional deposition of energy in the direct vicinity of the triggering EM cluster. The **M2** and **M4** match types are basically unaffected by pile-up.

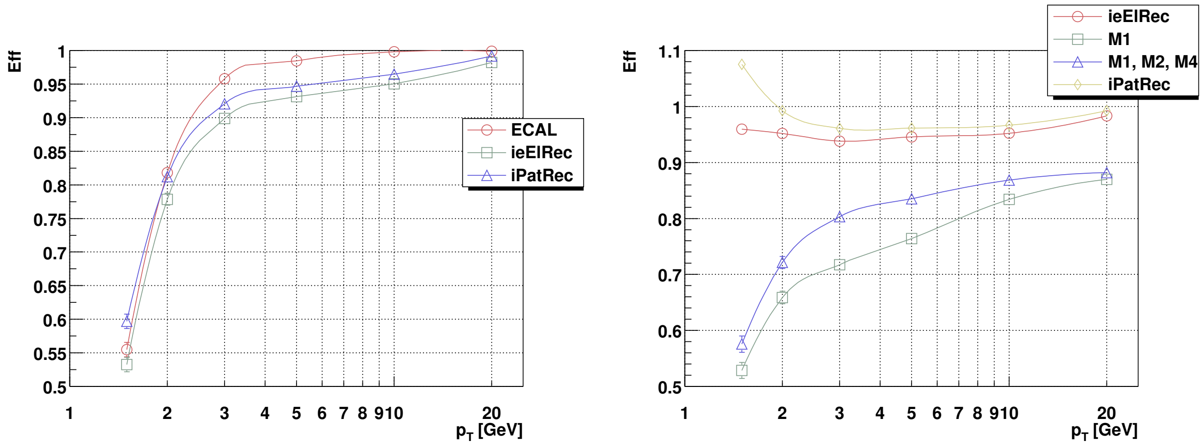

Figure 3.37: *Left:* absolute efficiencies of ECAL, `ieElRec` and `iPatRec` as a function of electron transverse momentum. *Right:* efficiencies, *relative* to the ECAL reconstruction efficiency, of `ieElRec`(irrespective of match type, for **M1** and for a union of **M1/2/4** match types) and `iPatRec`.

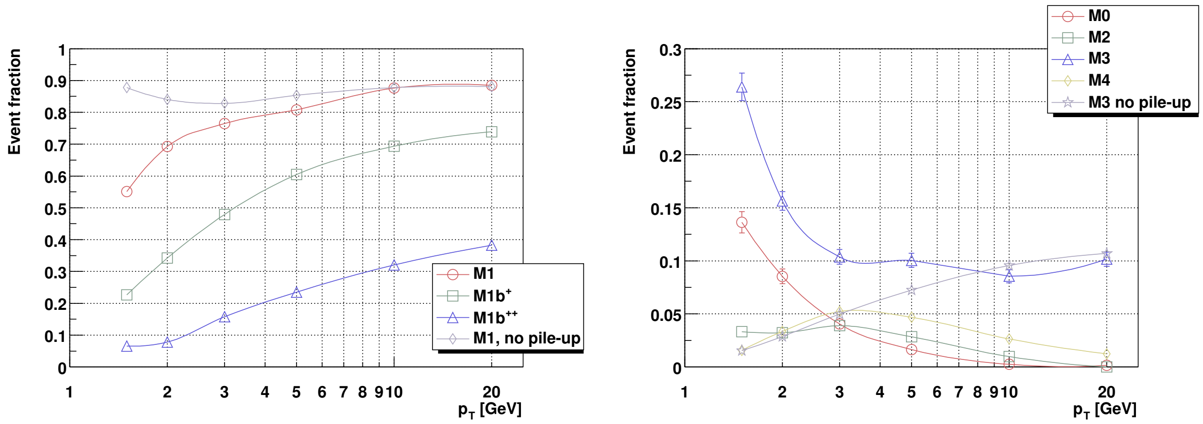

Figure 3.38: Relative fractions of ID/ECAL match types. Good matches are presented in the left plot (for comparison, **M1** *without* pile-up is also plotted) and poor ones in the right plot (with **M3** *without* pile-up added).

3.6.2 ECAL's E_T measurement

So far only event fractions and efficiencies have been considered without any concern for the underlying distributions of reconstructed p_T. The p_T distributions of tracks reconstructed in the ID differ from the ones without pile-up by migration of some well reconstructed electrons into poorer match types. This means that the p_T^{true}/p_T distributions of the **M0** and **M3** match types have more events in the central region and therefore a better mean value.

The normalised E_T/E_T^{true} distributions of the ECAL E_T measurement are presented in Fig:3.39. The distributions for the previously distinguished ID/ECAL match types support the statements made above about the inflow of energy into the area of ECAL to which an electron track projects to, and gives a more qualitative measure of the two effects. A statistical description of these distributions, in terms of mean values and rms's versus transverse energy, is presented in Fig:3.40. Returning to the **M1** match type, one can observe that its mean value is fixed at $E_T/E_T^{\text{true}} = 1$ which is basically just a cursor of the ECAL calibration that has been performed to account for the effects of high-luminosity pile-up. More interesting is the increase of noise, which manifests itself in a broadening of the distributions by 100 MeV.

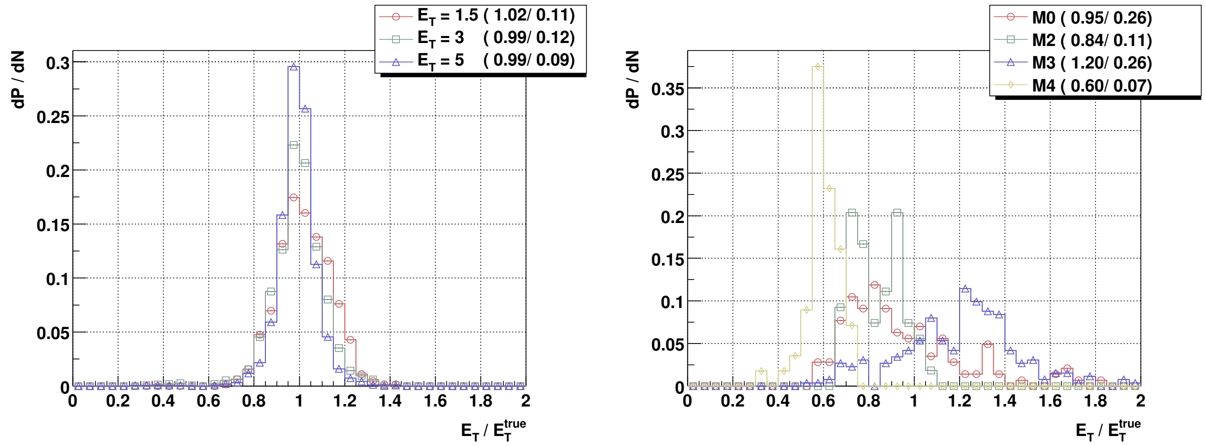

Figure 3.39: *Left:* normalised E_T/E_T^{true} distributions of **M1** ID/ECAL match type for $E_T = 1.5$, 3 and 5 GeV. *Right:* normalised E_T/E_T^{true} distributions of poor match types for $E_T = 2$ GeV. Both plots are labeled by mean values and rms's of distributions.

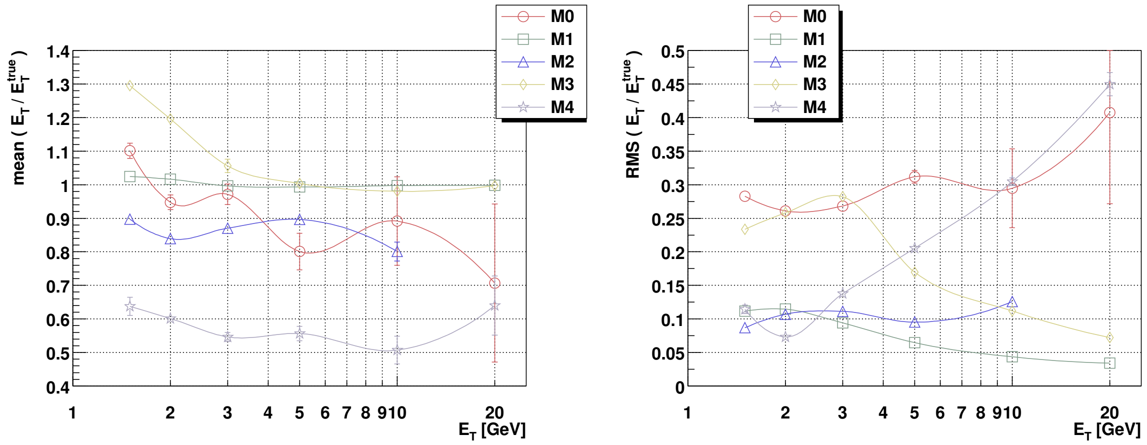

Figure 3.40: Mean values (left) and rms's (right) of E_T/E_T^{true} distributions. All ID/ECAL match types are presented. For **M1** the plotted value was obtained from a Gaussian fit in a range of $\pm 2 \times$ rms around the mean.